# In silico/in vitro screening and hit evaluation identified new phenothiazine antiprion derivatives

Zaccagnini  $L^{1\#}$ , Rossetti  $G^2$ , Tran  $HT^{1,4}$ , Salzano  $G^1$ , Gandini  $A^{1,3}$ , Colini Baldeschi  $A^1$ , Bolognesi  $ML^3$ , Carloni  $P^2$ , Legname  $G^{1*}$ 

- 1 Laboratory of Prion Biology, Department of Neuroscience, Scuola Internazionale Superiore di Studi Avanzati (SISSA), Via Bonomea 265, I-34136 Trieste, Italy
- 2 Institute for Advanced Simulations (IAS)-5/Institute for Neuroscience and Medicine (INM)-9, Forschungszentrum Jülich, 52428 Jülich, Germany
- 3 Department of Pharmacy and Biotechnology, Alma Mater Studiorum-University of Bologna , Via Belmeloro 6, I-40126 Bologna , Italy
- 4 VNUK Institute for Research and Executive Education The University of Danang, 158A Le Loi St., Da Nang, Vietnam
- # Current affiliation: Dementia Research Institute, University College London, Cruciform Building Gower street, London, United Kingdom
- \* Corresponding author. Laboratory of Prion Biology, Department of Neuroscience, Scuola Internazionale Superiore di Studi Avanzati (SISSA), via Bonomea 265, 34136 Trieste, Italy. Email: legname@sissa.it

Keywords: QSAR-model, prion, anti-prion agent, competition assay, RT-QuIC, chronic treatment

#### **Abstract**

Prion diseases or transmissible spongiform encephalopathies (TSEs) are a group of rare neurodegenerative disorders. TSEs are characterized by the accumulation of prions (PrPSc) that represent pathological isoforms of the physiological cellular prion protein PrPC. Although the conversion of PrPC to PrPSc is still not completely understood, blocking this process may lead to develop new therapies. Here, we have generated a pharmacophore model, based on anti-prion molecules reported in literature to be effective in phenotypic assay. The model was used to conduct a virtual screen of commercial compound databases that selected a small library of ten compounds. These molecules were then screened in mouse neuroblastoma cell line chronically infected with prions (ScN2a) after excluding neurotoxicity. 1 has been identified as the therapeutic hit on the basis of the following evidence: chronic treatments of ScN2a cells using 1 eliminate PrPSc loaded in both Western blotting analysis and Real-Time Quaking-Induced Conversion (RT-QuIC) assay. We also proposed the mechanism of action of 1 by which it has the ability to bind PrPC and consequentially blocks prion conversion. Herein we describe the results of these efforts.

## Introduction

In recent years, our understanding of the pathogenic mechanisms of neurodegenerative diseases has grown steadily. However, no effective therapies have yet been developed. These diseases are recognized as neurological protein misfolding disorders (PMDs) since they are associated with conformational changes of native proteins into disease-associated conformers [1]. PMDs include Alzheimer's disease, involving accumulation of misfolded amyloid  $\beta$  (A $\beta$ ) and tau, Parkinson's disease in which  $\alpha$ -synuclein aggregates, and prion diseases where the physiological form of the prion protein is converted into its pathological isoforms [2].

In the latter case, prior diseases or TSEs present as sporadic, inherited and infectious disorders [3]. Priors were long thought to be unique diseases. However, accumulating evidence suggests that in other PMDs other proteins might follow a similar mechanism of seeding, self-propagation and cell-to-cell spreading [4–8].

Neuropathological changes in TSEs are mainly gliosis, vacuolation and neuronal loss paralleled by cognitive and motor impairments [9,10]. TSEs include kuru, Creutzfeldt-Jacob disease, Gerstmann Sträussler-Scheinker syndrome and fatal familial insomnia in humans, bovine spongiform encephalopathy in cattle, scrapie in sheep and goats, and chronic wasting disease in elk, deer and other cervids [9]. The etiological agent is the scrapie prion protein (PrPSc), the abnormal, misfolded isoform of the PrPC [11]. PrPC is anchored to the cell surface through a C-terminal moiety of glycophosphatidyl-inositol or GPI [12]. Even though the two isoforms share the same primary sequence, they have several different biochemical and biophysical properties: PrPC is rich in  $\alpha$ -helices, is soluble in nonionic detergents and sensitive to protease K (PK) digestion while PrPSc is mostly rich in  $\beta$ -sheets, is insoluble in nonionic detergents and partially resistant to PK [13].

Although the conversion of PrP<sup>C</sup> to PrP<sup>Sc</sup> is still not completely understood, blocking this process may lead to the development of effective new therapies. Several studies have focused on the ability of small molecules to interfere with the conversion process, by either binding and stabilizing PrP<sup>C</sup> or blocking PrP<sup>Sc</sup> aggregation and accumulation [14–16]. A widely employed strategy has been the repositioning of compounds registered as antivirals [17], antimalarials [18,19], antifungals [20] and antidepressants [21]. Drug repositioning is the application of available drugs for treating conditions different from the original treatment purposes. By using this approach quinacrine (antimalarial) [18, 19], pentosan polysulfate (heparin mimetic) [22,23], doxycycline (antibiotic) [24,25] and flupirtine (analgesic) [26] were tested in human clinical trials, but with no encouraging results. Other approaches to develop anti-prion therapies rely on rational medicinal chemistry [26–28], multitarget approaches [29] and *in silico* methods [16,30]. However, most of the approaches attempted so

far have not resulted in molecules to progress into clinical investigations and all the identified drugs have inevitably failed [31]. Therefore, development of effective anti-prion small molecules that have drug-likeness and therapeutic potential remains a major challenge.

Toward this aim, our experimental program began with the generation of a pharmacophore model, based on anti-prion ligands reported to be effective in phenotypic assays, which was used to conduct a virtual screen of commercial compounds databases. This approach led to a small target-biased library, which was then screened in cellular model of the disease. Immortalized neuroblastoma (N2a) and hypothalamic (GT1) mouse cell lines chronically infected with different prion strains (RML and 22L) were used to measure anti-prion efficacy, after excluding neurotoxicity. 1 emerged as a therapeutic hit; it is able to eliminate PrP<sup>Sc</sup> after chronic treatments of N2a-RML cells as shown in both Western blotting analysis and Real-Time Quaking-Induced Conversion (RT-QuIC) assay. A mechanism by which prion conversion is blocked upon binding of 1 to PrP<sup>C</sup> is proposed. However, 1 suffered from poor solubility. We therefore carried out preliminary SAR studies on this compound, particularly focused on improving this physicochemical property.

### **Materials and Methods**

#### 2.1 Computational details

Two hundred compounds with known anti-prion activities ( $IC_{50}$ ) were identified by a literature search (Table S1) and included into 5 datasets, which are distinguished by inhibiting prion replication in cell lines and showing different incubation times in animal models of TSEs (Table S2). Our QSAR model uses Multiple Linear Regression (MLR) to obtain a linear relationship between the pIC<sub>50</sub> values against the molecular descriptors of these compounds. For this, we used ordinary least squares (OLS) algorithm in the QSARINS (QSAR-Insubria) software [32].

We calculated the molecular descriptors of the compounds using the PaDEL□descriptor code [33] and the Molinspiration (www.molinspiration.com) server.

We first eliminated the descriptors that possessed more than 95% of constant values and had more than 90% correlation using the QSARINS software [32]. The procedure led to 33 descriptors. It would be ideal to develop a QSAR model, which uses all combinations of available descriptors for the calculation of the models; however, the number of combinations is here so large that it is too computational demanding to include all models in the calculation. By applying genetic algorithm/multiple linear regressions (GA/MLR) technique, the most relevant descriptors for our

dataset were selected to build the final QSAR model. GA/MLR technique explores a broad range of possible combination of descriptors, searching for the best ones. This is done mimicking the natural selection; where every descriptor represents a gene, and a set of descriptors represent a chromosome. The fitness of a chromosome is related to the matching model performances. These increase with  $R^2$  (the correlation coefficient), with the quantity  $Q^2_{LOO}$  -  $R^2$  as close to zero (where  $Q^2_{LOO}$  is the  $R^2$  obtained by Leaving One value Out),  $Q^2_{LMO}$  -  $R^2$  as close to zero (where  $Q^2_{LMO}$  is the  $R^2$  obtained by Leaving Many values Out, around 30% of the data) and RMSE as close to zero (Root Mean Square Error is the standard deviation of the residuals, i.e. how far from the regression line data points are; RMSE tells you how concentrated the data is around the line of best fit).

Starting with a pool of chromosomes, small subsets of chromosomes are picked randomly, and the best become parents. Couples of parent chromosomes are then crossed at a random position (crossing-over), thus obtaining the offspring, whose chromosomes are combinations of the parent ones. If among the new chromosomes one or more of them outperform the fitness of the parent population, these chromosomes will replace the less performing. Repeating the aforesaid procedure many times, and introducing also random mutations (i.e. descriptor substitution) in the chromosomes, the result at the end of the procedure is a population of models with better performances than the models introduced at the beginning.

Our best final model features 5 descriptors. These are LogP, i.e. the partition coefficient of a compound between aqueous and lipophilic phases (usually octanol and water), compounds' Molecular Weight (MW), their number of Sulfur atoms (Nsulfur), their number of tricyclic scaffolds (Ntricyclic) and their molecular size, expressed in terms of an approximate diameter (D).

## 2.2 Chemistry

All the commercially available reagents and solvents were purchased from Sigma-Aldrich, TCI and Acros Organics, and used without further purification. Reactions were followed by analytical thin layer chromatography (TLC), on pre-coated TLC plates (layer 0.20 mm silica gel60 with a fluorescent indicator UV254, from Sigma-Aldrich). Developed plates were air-dried and analyzed under a UV lamp (UV 254/365 nm). CEM Discover SP focused microwave reactor was used for microwave mediated reactions. Nuclear magnetic resonance (NMR) experiments were run on Varian VXR 400 (400 MHz for <sup>1</sup>H, 100 MHz for <sup>13</sup>C). <sup>1</sup>H and <sup>13</sup>C NMR spectra were acquired at 300 K using chloroform (CDCl<sub>3</sub>), methanol (CD<sub>3</sub>OD), and dimethyl sulfoxide ((CD<sub>3</sub>)<sub>2</sub>SO) as solvents. Chemical shifts (δ) are reported in parts per million (ppm) relative to tetramethylsilane (TMS) as internal reference and coupling constants (J) are reported in hertz (Hz). The spin multiplicities are reported as s (singlet), d (doublet), t (triplet), q (quartet), and m (multiplet).

Compounds were named following IUPAC rules as applied by ChemBioDraw Ultra (version 14.0). Compounds purity was assessed by LC-MS using a SB-C18 RP column (100 x 2.1 mm I.D., 3.5  $\mu$ m) as the stationary phase and a mixture of 0.1% formic acid in water and 0.1% formic acid in acetonitrile (60/40, V/V), in isocratic mode at a flow rate of 100  $\mu$ L/min. Acquisition was performed by total ion current (TIC) and ESI+. 1 showed a purity  $\geq$ 98.1%. All the final 11-15 showed a purity  $\geq$ 95%.

- **2.2.1 Synthesis of 7-chloro-4-hydrazynilquinoline (16).** A suspension of 4,7-dichloroquinoline (500 mg) and hydrazine monohydrate 65% (2 eq) was irradiated in a sealed tube at 150 W for 5 min (T = 150°C, P = 200 psi, Power max = on). After cooling, the resulting solid was diluted with water, washed, and isolated by filtration. The final compound was purified through crystallization from ethanol, affording a pale yellow solid. Yield: 69%. <sup>1</sup>H-NMR (400 MHz, CD<sub>3</sub>OD):  $\delta$  8.41 (d, J = 5.6 Hz, 1H);  $\delta$  8.00 (d, J = 9.0 Hz, 1H);  $\delta$  7.80 (d, J = 1.8 Hz, 1H);  $\delta$  7.40 (dd, J = 9.0, 2.0 Hz, 1H);  $\delta$  6.99 (d, J = 5.6 Hz, 1H). <sup>13</sup>C-NMR (100 MHz, CD<sub>3</sub>OD):  $\delta$  158.55;  $\delta$  143.28;  $\delta$  140.69;  $\delta$  140.05;  $\delta$  128.23;  $\delta$  125.54;  $\delta$  120.16;  $\delta$  114.92;  $\delta$  99.67.
- **2.2.2 Synthesis of (Z)-2-(1-(2-(7-chloroquinolin-4-yl)hydrazono)ethyl)-10H-phenothiazine** (**compound 1**). To a solution of **16** (2.60 mmol) in ethanol (20 mL), 2-acetylphenothiazine (7.80 mmol) and acetic acid (2.5 mL) were added in sequence at room temperature. The solution was refluxed for 24h, and then evaporated under vacuum. The crude product was purified by column chromatography on silica gel (DCM/MeOH/NH<sub>3</sub> 9.2:0.8:0.08), affording **1** as a dark yellow solid. Yield: 81%. <sup>1</sup>H-NMR (400 MHz, DMSO- $d_6$ ):  $\delta$  8.68 (s, 1H);  $\delta$  8.40 (d, J = 8.7 Hz, 1H);  $\delta$  7.78-7.47 (m, 2H);  $\delta$  7.36 (t, J = 11.5 Hz, 2H);  $\delta$  7.24 (dd, J = 8.1, 1.8 Hz, 1H);  $\delta$  7.08 6.81 (m, 4H);  $\delta$  6.80 6.69 (m, 2H);  $\delta$  2.39 (s, 3H).

## 2.2.3 General procedure for the synthesis of compounds 11-15.

To a solution of **16** (0.3 mmol) in ethanol (3 mL), the corresponding phenothiazine derivatives **17-21** (0.3 mmol) and acetic acid (50  $\mu$ L) were added in sequence at room temperature. The solution was refluxed for 24h, and then evaporated under vacuum. All the final compounds were purified through column chromatography on silica gel (ethyl acetate/ethanol/toluene/NH<sub>3</sub> 6.8:0.2:3:0.02). (*E*)-2-(2-(1-(2-(7-chloroquinolin-4-yl)hydrazono)ethyl)-10H-phenothiazin-10-yl)-N,N-dimethylethan-1-amine (11). The title **11** was obtained as a yellow solid, according to the general procedure using **17**. Yield 50%. <sup>1</sup>H-NMR (400 MHz, CDCl<sub>3</sub>):  $\delta$  8.62 (s, 1H);  $\delta$  8.01 (s, 1H);  $\delta$  7.87 (d, J = 8.9, 1H);  $\delta$  7.55 (s, 1H);  $\delta$  7.48 (d, J = 5.4, 1H);  $\delta$  7.44 (dd, J = 8.9, 2.0, 1H);  $\delta$  7.35 (d, J =

7.9, 1H);  $\delta$  7.21-7.15 (m, 3H);  $\delta$  6.98-6.95 (m, 2H);  $\delta$  4.28 (s, 2H);  $\delta$  3.00 (s, 2H);  $\delta$  2.53 (s, 6H);  $\delta$  2.44 (s, 3H). <sup>13</sup>C-NMR (100 MHz, CDCl<sub>3</sub>):  $\delta$  206.87;  $\delta$  145.20;  $\delta$  144.72;  $\delta$  137.49;  $\delta$  135.13;  $\delta$  127.48;  $\delta$  127.15;  $\delta$  127.10;  $\delta$  125.89;  $\delta$  124.75;  $\delta$  122.74;  $\delta$  120.48;  $\delta$  115.79;  $\delta$  112.75;  $\delta$  102.53;  $\delta$  56.91;  $\delta$  53.38;  $\delta$  45.38;  $\delta$  45.02;  $\delta$  30.88;  $\delta$  29.66;  $\delta$  24.42;  $\delta$  22.65;  $\delta$  14.08;  $\delta$  12.61.

(E)-3-(2-(1-(2-(7-chloroquinolin-4-yl)hydrazono)ethyl)-10H-phenothiazin-10-yl)-N,N-(E)-3-(E)-3-(E)-10

dimethylpropan-1-amine (12). The title 12 was obtained as a yellow solid, according to the general procedure using 18. Yield 35%. <sup>1</sup>H-NMR (400 MHz, CDCl<sub>3</sub>): δ 8.63 (s, 1H); δ 7.99 (s, 1H); δ 7.77 (d, J = 8.8, 1H); δ 7.43 (d, J = 7.1, 3H); δ 7.29 (d, J = 7.9, 1H); δ 7.24 (s, 1H); δ 7.15 (dd, J = 15.8, 8.0, 3H); δ 6.92 (d, J = 7.0, 2H); δ 4.03 (t, J = 6.3, 2H); δ 2.66-2.48 (m, 2H); δ 2.39 (s, 3H); δ 2.28 (s, 6H); δ 2.15-1.99 (m, 2H). <sup>13</sup>C-NMR (100 MHz, CDCl<sub>3</sub>): δ 206.87; δ 145.20; δ 144.72; δ 137.49; δ 135.13; δ 127.48; δ 127.15; δ 125.89; δ 124.75; δ 122.74; δ 120.48; δ 115.79; δ 112.75; δ 102.53; δ 56.91; δ 53.38; δ 45.38; δ 45.02; δ 30.88; δ 29.66; δ 29.32; δ 24.42; δ 22.65; δ 14.08; δ 12.61.

(E) - 2 - (1 - (2 - (7 - chloroquinolin - 4 - yl)hydrazono) ethyl) - 10 - (2 - (piperidin - 1 - yl)ethyl) - 10 H - (2 - (piperidin - 1 - yl)ethyl) - 10 H - (2 - (piperidin - 1 - yl)ethyl) - 10 H - (2 - (piperidin - 1 - yl)ethyl) - 10 H - (2 - (piperidin - 1 - yl)ethyl) - 10 H - (2 - (piperidin - 1 - yl)ethyl) - 10 H - (2 - (piperidin - 1 - yl)ethyl) - 10 H - (2 - (piperidin - 1 - yl)ethyl) - 10 H - (2 - (piperidin - 1 - yl)ethyl) - 10 H - (2 - (piperidin - 1 - yl)ethyl) - 10 H - (2 - (piperidin - 1 - yl)ethyl) - 10 H - (2 - (piperidin - 1 - yl)ethyl) - 10 H - (2 - (piperidin - 1 - yl)ethyl) - 10 H - (2 - (piperidin - 1 - yl)ethyl) - 10 H - (2 - (piperidin - 1 - yl)ethyl) - 10 H - (2 - (piperidin - 1 - yl)ethyl) - 10 H - (2 - (piperidin - 1 - yl)ethyl) - 10 H - (2 - (piperidin - 1 - yl)ethyl) - (2 - yl)ethyl)ethyl - (2 - yl)ethyl -

*phenothiazine* (*13*) The title **13** was obtained as a yellow solid, according to the general procedure using **19**. Yield 22%. <sup>1</sup>H-NMR (400 MHz, CDCl<sub>3</sub>): δ 8.55 (d, J = 5.2 Hz, 1H); δ 7.94 (d, J = 1.9 Hz, 1H); δ 7.75 (d, J = 8.9 Hz, 1H); δ 7.46 (d, J = 1.6 Hz, 1H); δ 7.41-7.32 (m, 2H); δ 7.32-7.25 (m, 1H); δ 7.18-7.05 (m, 3H); δ 6.92-6.88 (m, 2H); δ 4.12-4.06 (m, 2H); δ 3.70-3.67 (m, 4H); δ 2.82-2.79 (m, 2H); δ 2.55-2.53 (m, 3H); δ 2.36 (s, 3H); δ 2.01 (s, 1H); δ 1.23 (t, J = 7.1 Hz, 2H). <sup>13</sup>C-NMR (100 MHz, CDCl<sub>3</sub>): δ 150.54; δ 148.22; δ 147.68; δ 146.90; δ 144.93; δ 144.55; δ 137.38; δ 135.32; δ 127.90; δ 127.50; δ 127.39; δ 127.05; δ 126.46; δ 125.87; δ 124.08; δ 122.72; δ 120.92; δ 120.45; δ 115.92; δ 115.46; δ 112.56; δ 102.35; δ 66.89; δ 55.93; δ 54.02; δ 45.98; δ 12.69.

(*E*)-4-(2-(2-(1-(2-(7-chloroquinolin-4-yl))hydrazono)ethyl)-10H-phenothiazin-10-

yl)ethyl)morpholine (14) The title 14 was obtained as a dark yellow solid, according to the general procedure using 20. Yield 91%. <sup>1</sup>H-NMR (400 MHz, CDCl<sub>3</sub>): δ 8.53 (d, J = 5.0, 1H); δ 8.01 (d, J = 2.0, 1H); δ 7.94 (d, J = 8.9, 1H); δ 7.51 (d, J = 1.6, 1H); δ 7.48-7.40 (m, 2H); δ 7.37 (dd, J = 8.0, 1.7, 1H); δ 7.22-7.14 (m, 3H); δ 6.98-6.94 (m, 2H); δ 4.15 (t, J = 6.7 Hz, 2H); δ 3.75-3.73 (m, 4H); δ 2.87 (t, 2H); δ 2.67-2.56 (m, 4H); δ 2.50 (s, 3H). <sup>13</sup>C-NMR (100 MHz, CDCl<sub>3</sub>): δ 150.54; δ 148.22; δ 147.68; δ 146.90; δ 144.93; δ 144.55; δ 137.38; δ 135.32; δ 127.90; δ 127.50; δ 127.39; δ 127.05; δ 126.46; δ 125.87; δ 124.08; δ 122.72; δ 120.92; δ 120.45; δ 115.92; δ 115.46; δ 112.56; δ 102.35; δ 66.89; δ 55.93; δ 54.02; δ 45.98; δ 12.69.

(*E*)-2-(1-(2-(7-chloroquinolin-4-yl)hydrazono)ethyl)-10-(2-(4-methylpiperazin-1-yl)ethyl)-10H-phenothiazine (*15*) The title **15** was obtained as a dark yellow solid, according to the general procedure using **21**. Yield 37%. <sup>1</sup>H-NMR (400 MHz, CDCl<sub>3</sub>):  $\delta$  8.59 (s, 1H);  $\delta$  7.98 (s, 1H);  $\delta$  7.83 (d, J = 8.5, 1H);  $\delta$  7.49 (s, 1H);  $\delta$  7.42-7.32 (m, 2H);  $\delta$  7.30 (d, J = 8, 1H);  $\delta$  7.18-7.11 (m, 3H);  $\delta$ 

6.94-6.92 (m, 2H);  $\delta$  4.12 (t, J = 6.8, 2H);  $\delta$  2.87 (t, J = 6.8, 2H);  $\delta$  2.71-2.60 (m, 6H);  $\delta$  2.38 (s, 3H);  $\delta$  2.35 (s, 3H)  $\delta$  1.24-1.18 (m, 2H). <sup>13</sup>C-NMR (100 MHz, CDCl<sub>3</sub>):  $\delta$  142.36;  $\delta$  142.03;  $\delta$  134.86;  $\delta$  132.79;  $\delta$  124.94;  $\delta$  124.85;  $\delta$  124.53;  $\delta$  123.37;  $\delta$  121.67;  $\delta$  120.19;  $\delta$  117.96;  $\delta$  112.96;  $\delta$  110.09;  $\delta$  99.81;  $\delta$  52.54;  $\delta$  52.12;  $\delta$  50.14;  $\delta$  43.46;  $\delta$  42.83; 10.24.

## 2.2.4 Kinetic Solubility Studies.

A variation of a previously reported method was employed to determine the compounds' solubility in buffer at pH 7.4 [33]. Briefly, 10 mM DMSO stock solutions of **1** and derivatives **11-15** were diluted to 200 or 600  $\mu$ M in PBS (pH 7.4). The mixtures were stirred for 30 min, filtered, and then injected onto a Jasco Corporation PU-1585 HPLC system (Solvent system: 73% H<sub>2</sub>O/27% MeCN + 0.1% trifluoroacetic acid; Column: Kinetex® 5 $\mu$ m EVO C18 100 Å, 150 x 4.6 mm; UV: 254 nm). A 10 mM stock solution was prepared by completely dissolving test compounds in DMSO. This solution was diluted to five known concentration solutions in MeCN. Each solution was analyzed by HPLC, and a calibration curve was plotted using the peak areas from the standard concentrations. The equilibrium solubility of test compounds was determined by quantifying the concentration of test solutions against the calibration curve (Figure S3). Experiments were run in triplicate, and results were tabulated and reported as mean  $\pm$  standard deviation (Table S5).

## 2.3 Biological evaluation

#### 2.3.1 Cell culture

Mouse neuroblastoma cell line, either non-infected (N2a) or chronically infected with Rocky Mountain Laboratory (RML) or with 22L prion strains (ScN2a) were grown in Minimal Essential Medium (MEM)-1% L-glutamax complemented with 10% fetal bovine serum (FBS), 1% non-essential amino acids (NEAA), and 1% penicillin-streptomycin.

Immortalized mouse hypothalamic neurons (GT1) and chronically infected ScGt1 cells, with both RML and 22L prion strains, were grown in Dulbecco's modified Eagle's medium (DMEM)-1% GlutaMAX supplemented with 10% FBS and 1% penicillin-streptomycin.

All cell lines were cultivated in 25 cm<sup>2</sup> flasks at 37 °C under 5% CO<sub>2</sub> or in 10 cm<sup>2</sup> Petri dishes.

## 2.3.2 Compounds

All the compounds were dissolved in 100% dimethyl sulfoxide (DMSO), to a 10 mM stock solution. From these stock solutions, intermediate dilutions were prepared as needed. For cell treatment, stock solutions were further diluted in 100% ethanol (EtOH) to a final concentration of 1 mM. Each molecule was then diluted in cell culture medium. In the cell medium, the final

concentration of DMSO was never above 0.1%. Detailed treatment conditions are provided in following methods. Mock controls were treated with vehicle only under the same conditions.

#### 2.3.3 Assessment of cell viability

N2a, N2a chronically infected with RML or 22L prion strain (ScN2a), GT1 and GT1 chronically infected with RML or 22L prion (ScGT1) cells, were maintained in culture and grown to 80% confluence. The medium was changed and the cells were detached.

The cell density was determined by cell counting using ScepterTM 2.0 Cell Counter (Millipore). The cell density was adjusted to  $2.5 \times 10^4$  cell/mL with MEM (N2a, ScN2a) or  $3 \times 10^4$  with DMEM (GT1, ScGT1).

The cell suspension was added to each well of a 96-well, tissue culture-treated, clear bottom, plate (Costar) and the cells were allowed to settle for 1 day at 37 °C under 5% CO<sub>2</sub> prior to the addition of the compounds.

Each compound (dissolved in EtOH) was diluted in the cell medium to a final concentration of 0.1, 1 and 10  $\mu$ M. After 24 h, cell culture medium was removed and replaced by compound-containing medium.

The plate was incubated at 37 °C under 5% CO<sub>2</sub> for 5 days.

## 2.3.3.1 MTT assay

The 3-(4,5-dimethylthiazol-2-yl)-2,5-diphenyltetrazolium bromide (MTT, SIGMA) was diluted in phosphate buffer solution (PBS) to a working dilution of 5 mg/mL.

The medium was then removed, and the cells were incubated with the MTT solution for 3 h at 37 °C under 5% CO<sub>2</sub>.

After incubation, a solution of DMSO/2-Propanol (1:1) was added to each well and the plate was kept at room temperature (RT) for 30 min before reading. Absorbance was measured at OD = 590 nm by using a Spectramax M5 (Molecular Devices).

## 2.3.3.2 Cell counting KIT-8

Ten  $\mu M$  of CCK-8 solution (ST-8 [2-(2-methoxy-4-nitrophenyl)-3-(4-nitrophenyl)-5-(2,4-disulfophenyl)-2H-tetrazolium, monosodium salt) (Dojindo Labroatories) were added to each well of the plate.

The plate was then incubated for 4 hours in the humidified incubator (e.g., at 37°C, 5% CO<sub>2</sub>). After that, the absorbance was measured at 450 nm using the microplate reader (Spectramax M5, Molecular Devices).

### 2.3.3.3 Calcein assay

Ten  $\mu$ L of 2.5  $\mu$ M calcein-AM were added, and the plates were incubated at 37°C for 30 min. Fluorescence emission intensity was quantified using a SpectraMax M5 fluorescence plate reader, excitation/emission ratio equal to 492/525 nm.

# 2.3.4 PrPSc and PrPC detection in cell lysates by western blotting

After the treatment with compounds, the amount of PK-resistant  $PrP^{Sc}$  was measured in ScN2a and ScGT1 treated with 1  $\mu$ M of concentration of each compound or then with a titration of 1. After 4 days of treatment, the accumulation of PrP protein was detected by immunoblotting of lysed cells before and after PK digestion.

### 2.3.4.1 Cell lysates

After removing the medium and washing the cells with PBS, lysis buffer (10 mM Tris-HCl pH 8.0, 150 mM NaCl, 0.5% nonidet P-40, 0.5% deoxycholic acid sodium salt) was added to the flasks/dishes, then the cells were detached using a cell scraper (Falcon) and the lysates were collected and pelleted by centrifugation in a bench microfuge (Eppendorf).

## 2.3.4.3 PK digestion

Two hundred and fifty  $\mu g$  or 500  $\mu g$  of protein were digested with 10  $\mu g$  of PK (Roche) for 1 h at 37 °C.

The reaction was arrested with 2 mM of phenylmethylsulphonyl fluoride (PMSF, SIGMA) and the PK-digested cell lysates were centrifuged at 55000 rpm for 75 min at 6°C in an ultracentrifuge (Beckman Coulter).

After the centrifugation, the supernatants were discarded, and the pellets were re-suspended in 2X or 5X sample loading buffer (125 mM Tris HCl, pH 6.8, 10% 2-mercaptoethanol, 4% SDS, 0.2% bromophenol blue, 20% glycerol and 200mM DTT) and boiled for 10 min at 100 °C. An amount equal to 30 µg of total proteins was used for the non-PK-digested samples, boiled for 10 min.

#### 2.3.4.4 SDS-PAGE and immunoblotting

Samples were loaded onto a 12% Tris-Glycine SDS-PAGE gel for protein separation, then they were transferred to a nitrocellulose membrane (GE Healthcare).

The membrane was blocked with 5% non-fat milk in TBST (Tris 200 mM, NaCl 1.5 mM, 1% Tween-20) for 1 hour at RT and incubated with 1  $\mu$ g/mL anti-PrP Fab W226, diluted in blocking

solution, overnight at 4 °C. After washes with TBST, the membrane was incubated for 1 h a RT with secondary antibody (goat anti-mouse IgG F(Ab)2 conjugated with horseradish peroxidase (HRP), DAKO) diluted 1:1000 in blocking solution. After washes, the signal was detected using enhanced chemiluminescent system (ECL, Amersham Biosciences) and Uvitec Alliance (Cambridge).

Densitometric analysis was performed using Uviband Analysis Software.

Data are expressed as mean  $\pm$  SD, and the values of the controls are adjusted to 100%.

Each experiment was performed in triplicate.

# 2.3.4.5 PrP<sup>C</sup> detection in cell lysates by western blotting

The same treatment conditions reported above were used for non-infected N2a and GT1 cells. After 4 days of drug treatment, the amount of  $PrP^{C}$  was measured by immunoblotting of lysed cells. Thirty  $\mu g$  of total proteins were used for the analysis. Same protocol as above was used, without PK digestion step. Each experiment was performed in triplicate.

# 2.3.4.6 PrPSc quantification by ELISA assay

PK digestion of cell lysates was performed as described above. After ultracentrifugation, pellets were dissolved and denatured in 50  $\mu$ L of 8 M guanidine hydrochloride (GdnHCl) in coating buffer (0.1 M sodium bicarbonate, pH 8.2) for 1 h and diluted into 500  $\mu$ L of coating buffer.

Twenty  $\mu$ L of the suspension were transferred to 96-well MaxiSorp ELISA plates (Nunc), with each well containing 180  $\mu$ L of coating buffer and the plates were sealed and incubated overnight at 4 °C. To increase the immuno-reactivity of PrPSc, coated proteins were denatured in situ. Fifty  $\mu$ L of 8 M GdnHCl were added to each well and incubated for 10 min at room temperature. The ELISA plates were washed three times with TBST and blocked with 200  $\mu$ L of 3% BSA in TBS (20 mM Tris-HCl, 137 mM NaCl, pH 7.5) for 1 h at 37 °C. After three washes with TBST, the plates were incubated with anti-PrP antibody W226 (1.5  $\mu$ g/mL) in 1% BSA/TBS, at 37 °C for 2 h. After seven washes with TBST, goat anti-mouse IgG Fab conjugated to HRP diluted 1:1000 in 1% BSA/TBS was added to the plates and incubated at 37 °C for 1 h. Again, plates were washed seven times with TBST, and then developed with 1-step TMB (3,3',5,5'- tetramethylbenzidine) Turbo ELISA HRP substrate (Pierce).

The reaction was stopped by the addition of 2 M sulfuric acid to the plates. Absorbance at 450 nm was measured using a microplate reader (VersaMax, Molecular Devices). Dose-response curves and IC<sub>50</sub> values were computed using IGOR (Demo Version 6.32).

## 2.3.5 Recombinant full-length mouse PrP production and purification

The mouse construct encoding for full-length PrP was expressed in competent BL21 Rosetta2 (DE3) cells *Escherichia coli* (Stratagene).

Freshly transformed overnight culture was inoculated into Luria Bertani (LB) medium and 100  $\mu$ g/mL ampicillin and 30  $\mu$ g/mL chloramphenicol. At 0.8 OD600 expression was induced with isopropyl b-D galactopyranoside (IPTG) to a final concentration of 1 mM. Cells were grown in a BioStat-B plus fermentor (Sartorius). The cells were lysed by a homogenizer (PandaPLUS 2000) and the inclusion bodies were suspended in buffer containing 25 mM Tris-HCl, 5 mM EDTA, 0.8% TritonX100, pH 8, and then in bi-distilled water several times.

Inclusion bodies containing MoPrP (23-231) were dissolved in 5 volumes of 8 M guanidine hydrochloride (GdnHCl), loaded onto pre-equilibrated HiLoad 26/60 Superdex 200-pg column, and eluted in 25 mM Tris–HCl (pH 8.0), 5 mM ethylenediaminetetraacetic acid, and 5 M GdnHCl at a flow/rate of 1.5 mL/min. Protein refolding was performed by dialysis against refolding buffer [20 mM sodium acetate and 0.005% NaN3 (pH 5.5)] using a Spectrapor membrane (molecular weight, 10000). Purified protein was analyzed by SDS-polyacrylamide gel electrophoresis under reducing conditions and Western blot.

## 2.3.6 Competition assay

A mix of recombinant mouse full length PrP (MoPrP(23-231)) and **1** was incubated at 37 °C in 350 rpm of shaking for 30 minutes.

The mixes were different:

•  $PrP : \mathbf{1} = 1:1 = 1 \mu M : 1 \mu M$ 

• PrP :  $\mathbf{1} = 2:1 = 2\mu M : 1\mu M$ 

• PrP:  $\mathbf{1} = 1:2 = 0.5 \, \mu \text{M} : 1 \, \mu \text{M}$ 

• PrP:  $\mathbf{1} = 1.5 = 0.2 \,\mu\text{M} : 1\mu\text{M}$ 

After 1 hour, the mix and the other treatments (1 alone) were centrifuged at 2000 rpm in Nanosep centrifugal device (Merk) with Omega membrane 3 kDa to pass the whole solution through. These tubes are permeable to 1 (416.93 Da) but not to the PrP (25 kDa) and to the PrP-1 complex (Figure S1).

The mix and the other treatments were added to the cells as a normal treatment for 4 days. Then the cells were lysed, and results observed by SDS-page and RTQuIC.

#### 2.3.7 RT-QuIC procedure

After purification, aliquots of the recombinant PrP (MoPrP(23-231)) were stored at -80 °C in 10 mM phosphate buffer (pH 5.8). Before each test, the protein solution was allowed to thaw at room temperature and filtered using Millex-GV filter 0.22  $\mu$ m (Millipore).

The final reaction volume was 100  $\mu$ L loaded into the plate (ViewPlate-96 F TC/50x1B, Perkin Elmer) and the reagents (Sigma) were concentrated as follow: 150 mM NaCl, 0.002% SDS, 1X PBS, 1 mM EDTA, 10  $\mu$ M ThT and 0.2 mg MoPrP(23-231) ml-1.

The seed consists of sonicated ScN2a-RML cells. Before the sonication the cells were collected in  $100 \mu l$  of PBS 1X, after the sonication the sample was quantified using the BCA assay, in order to use it as a seed (1  $\mu g$  of the protein).

After the addition of 10  $\mu$ L of seed, the plate was sealed with a sealing film (Perkin Elmer) and inserted into a FLUOstar OPTIMA microplate reader (BMG Labtech). The plate was shaken for 1 minute at 600 rpm (double orbital) and incubated for 1 minute at 45 °C.

Fluorescence readings (480 nm) were taken every 30 minutes (30 flashes per well at 450 nm). Given the rapid response, a specific threshold was set to decrease the likelihood of false positives. A sample was considered positive if the mean of the highest two fluorescence values (AU) of the replicates was higher than 10000 AU and at least two out of three replicates crossed the threshold that was set at 30 hours. This reaction cutoff was established because in all the experiments there were wells only with MoPrP(23-231) and in these cases no positive RT-QuIC reactions were observed until after 30 hours.

## 2.3.8 Immunofluorescence of fixed cells, the surface staining

N2a cells were seeded to semi-confluence in each well of a 24-well plate containing a poly-lysine coated coverslip and an appropriate culture medium coverslip for 24 hours.

After one day of incubation, the cells were put on ice for 15 minutes.

Then the cells were stained with the primary antibody (W226 1:200) in culture medium for 20 minutes, always in ice. After this time, the medium was removed, and the cells were washed 2 times with PBS.

The cells were then removed from the ice and were fixed using 4 % of paraformaldehyde (PFA) for 20 minutes. The PFA was discharged and the cells were washed 3 times for 5 minutes with PBS.

Blocking buffer, consisting of 7% Normal Goat Serum (NGS) in PBS, was added to the cells for 1 hour at room temperature. After the blocking, the cells were incubated with a secondary antibody (Goat anti-mouse [G $\alpha$ Mo]-AlexaFluor488, Life Technologies) diluted 1:1000 in the incubation buffer (1% NGS, 0.02% triton-100 in PBS) for 1 hour at room temperature in the dark.

After 2 washes of 5 minutes in PBS, the cells were incubated with 0.1-1  $\mu$ g/ml of DAPI (Life Technologies) in PBS-T for 5 minutes.

The cells were washed 3 times in PBS for 5 minutes and then the coverslips were mounted with a drop of Fluoromount-G (Invitrogen). The coverslips were sealed with nail polish to prevent drying and movement under the microscope.

Images were acquired with C1 confocal microscope (Nikon). FITC filter was used for detection of PrP specific staining, while Dapi specific staining was acquired with 500 nm filter.

#### **Results**

## 3.1 In silico screening

## 3.1.1 QSAR model

We first constructed a list of ca. 200 compounds with known anti-prion activities ( $IC_{50}$ ) by collecting data from 14 publications (Table S1). The compounds were divided into 5 datasets depending on the type of cell line used in the assays and their incubation time (see Table S2). For each dataset, we generated a QSAR model. Here we present the best model (according to criteria specified in the Materials and Methods section and below) across the five datasets: this is the QSAR model based on the ScN2a cell line dataset, see below.

For each compound in the dataset, constitutional, topological, geometric, electrostatic, hydrophobic and steric descriptors were generated. Plus the drug-likeness (Lipinski's rule of 5) [34] was calculated by using PaDEL\(\top\) descriptor code [35] and the Molinspiration webserver (www.molinspiration.com).

Several of these descriptors were correlated with each other or did not display sufficient variability within the dataset and were therefore discarded (see Material and Methods section). Next, the most relevant descriptors for our dataset were identified by applying genetic algorithm/multiple linear regressions (GA/MLR) technique. This is commonly used with experimentally measured pIC50 [36][37][38].

The resulting best QSAR model was found to depend on the following descriptors: the compounds' LogP (logarithm of partition coefficient of the molecule in a octanol/water system), their Molecular Weight (MW), their number of Sulfur atoms (Nsulfur), their number of tricyclic scaffolds (Ntricyclic) and their molecular size, expressed in terms of an approximate diameter (D).

The best QSAR model, reporting predicted  $pIC_{50}$  values as a function of the five descriptors, is shown in Figure 1.

The expression of  $pIC_{50}$  reads:

$$pIC_{50} = 0.2344(0.066)LogP \qquad 0.0047(0.008)MW + 0.3597(0.1135)NSulfur + 0.6237(0.2450)NTricyclic + 0.2278(0.0242)D + 2.6812$$
 
$$n=38, R^2=0.80, R^2adj=0.77, s=0.34, F=26.06, Q^2loo=0.72, Q^2lmo, 30\%=0.71, R^2-R^2adj=0.031$$

where n is the number of compounds of the training set, s is standard error of estimate, F is variance ratio,  $R^2$  is the coefficient of determination,  $R^2$ adj is an "adjusted"  $R^2$  based on the number of independent variables in the model: it is indicative of the convenience to add a new descriptor to the model. Our value is comparable with that of  $R^2$ . Therefore, the model exhibits no overfitting. In other words, it presents a good fit with minimum number of descriptors.  $Q^2_{LOO}$  (Leave One Out) and  $Q^2_{LMO}$  (leave many out) are values of  $R^2$  calculated by removing randomly one or 30% of the values. The criterion based on  $Q^2_{LMO}$  is particularly important as it introduces a significant perturbation on the data in contrast to  $Q^2_{LOO}$ . Both values should be rather close to  $R^2$  for the model to be robust. This is the case here.

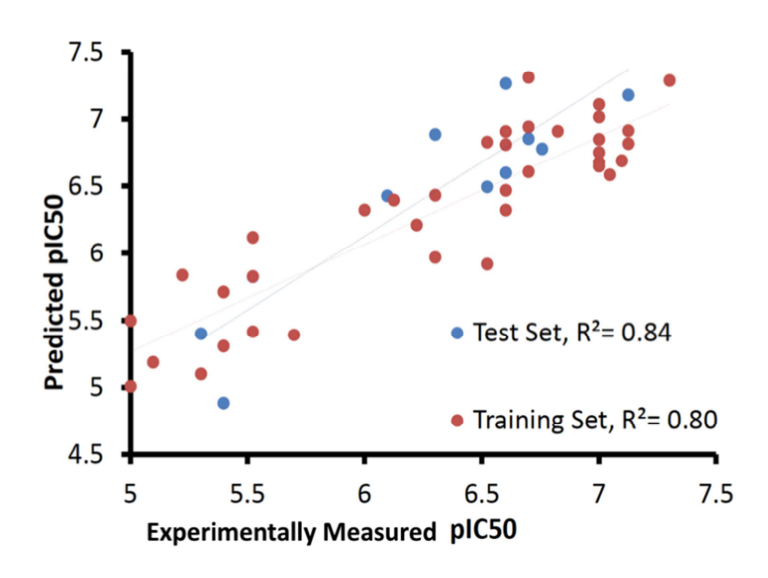


Figure 1. QSAR model obtained by QSARIN software on ScN2a cell line

## 3.1.2 Virtual screening

The values of IC<sub>50</sub> were calculated for 2029 compounds using our QSAR model. These compounds were identified by screening the Zinc database (http://zinc.docking.org) according to the following criteria (i) they follow the Lipinski rule of 5; (ii) they are within the Applicability Domain of our proposed model; (iii) they contain a moiety similar to chloroquine. The compounds with the largest values of predicted IC<sub>50</sub> were selected for the binding assays (Figure 2).

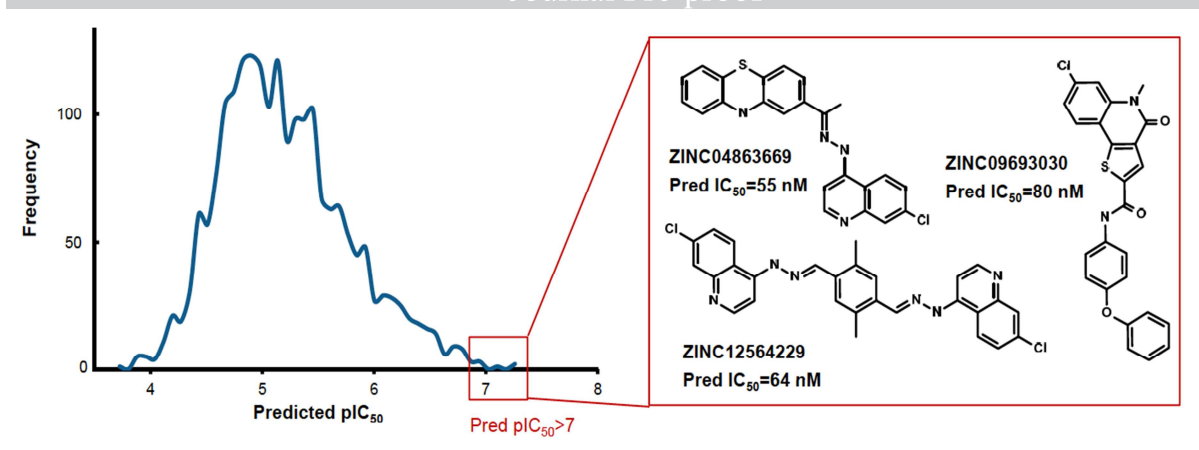


Figure 2. Distribution of the predicted pIC<sub>50</sub> among the 2029 compounds extracted from the ZINC database. Example of compounds with highest predicted pIC<sub>50</sub> is highlighted in the red box.

A small set of 10 molecules (**1-10** in Figure 3) was selected, spanning different bicyclic and tricyclic scaffolds (e.g. quinoline, acridine and phenothiazine derivatives).

## 3.2 In vitro screening

The *in vitro* screening of **1-10** was performed using the N2a cell line chronically infected with RML prion strain. The ability of all compounds to reduce  $PrP^{Sc}$  level was determined by Western blotting followed by densitometry of the PK resistant  $PrP^{Sc}$ . The first assessment of the compounds was performed at 1  $\mu$ M concentration.

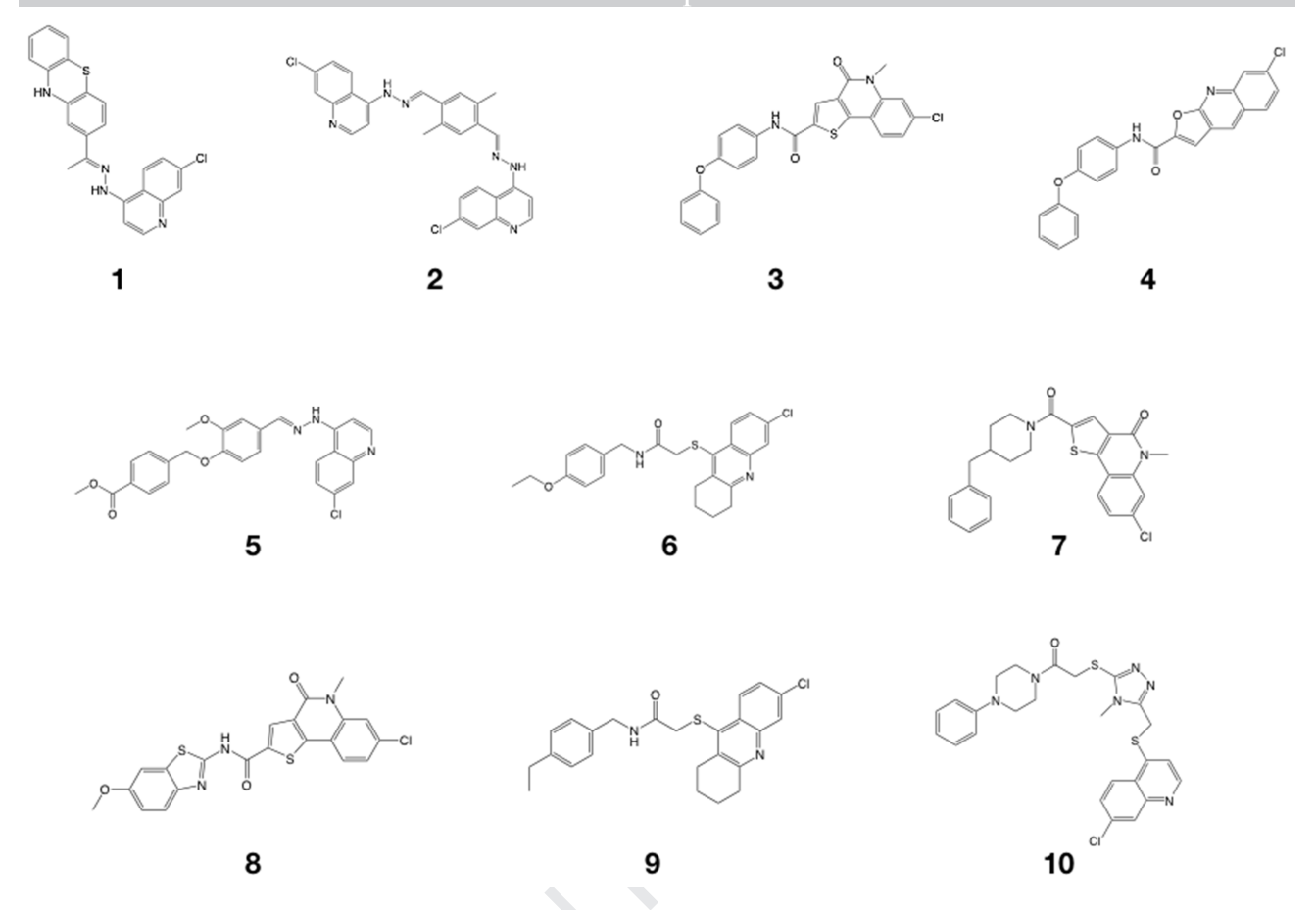


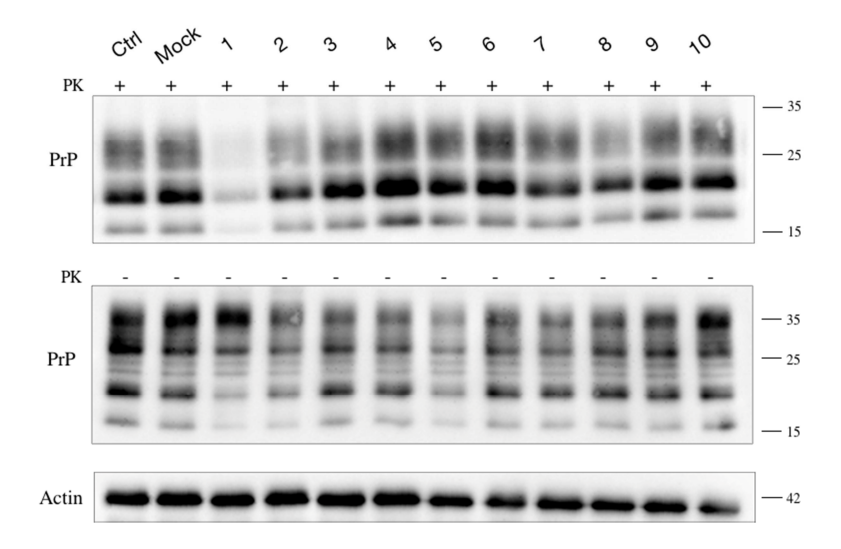
Figure 3. Chemical structure of the 10 selected compounds

# 3.2.1 Inhibition of $PrP^{Sc}$ replication at a concentration of 1 $\mu M$

Before starting the evaluation of the anti-prion potential of 1-10, we determined their effects on cell viability using three different assays: MTT assay, CCK-8 kit, calcein assays and setting a toxicity threshold of 80% [39]. Positively, no toxicity was observed in the assays (Table S3). Then, their ability to reduce the level of the resistant PrP<sup>Sc</sup> in prion-infected cells was determined by Western blotting densitometric analysis. Relative amounts of PK-resistant PrP<sup>Sc</sup> were measured comparing to untreated ScN2a-RML cell lysates.

Molecules **3**, **4**, **5**, **7**, **8** and **10** in four independent experiments did not decrease the levels of PrP<sup>Sc</sup>. **2** and **9** showed mild anti-prion efficacy, while the treatment of ScN2a-RML cells with **1** resulted in harboring 35% of PK-resistant PrP<sup>Sc</sup> (Figure 4A-B).

 $\mathbf{A}$ 



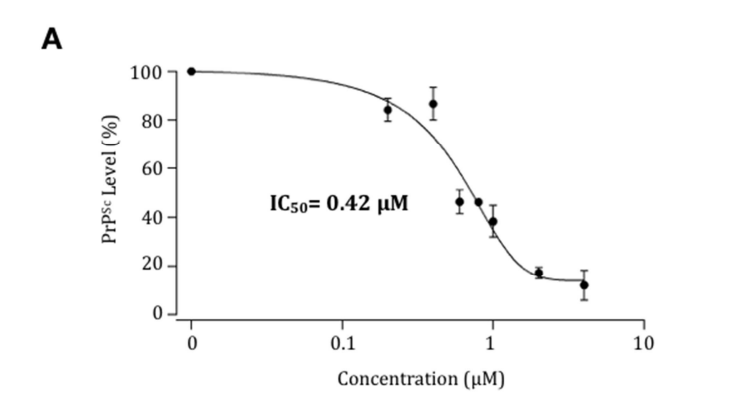
В		
Compound	-PK	+PK
Ctrl	100	100
Mock	$92.4 \pm 7.2$	$94.0 \pm 8.1$
1	$55.7 \pm 6.3$	$35.6 \pm 8.8$
2	$63.8 \pm 6.0$	$70.9 \pm 17.3$
3	$92.5 \pm 8.9$	$94.4 \pm 12.8$
4	$92.6 \pm 11.1$	$108.6 \pm 19.3$
5	$95.6 \pm 12.1$	$82.3 \pm 18.0$
6	$109.5 \pm 20.4$	$101.7 \pm 3.1$
7	$99.6 \pm 20.7$	$82.4 \pm 11.8$
8	$69.1 \pm 3.5$	$85.4 \pm 12.1$
9	$83.5 \pm 14.0$	$77.1 \pm 17.3$
10	$85.8 \pm 11.6$	$88.0 \pm 19.9$

Figure 4. Anti-prion effect evaluation of all compounds at 1  $\mu$ M of concentration. (A) Western blot of ScN2a-RML cell lysates depicting the presence or absence of prions following the treatment with the compounds before (down) or after (up) PK digestion. The proteinase-K digested cell lysates were detected with W226 anti-PrP monoclonal antibody. Bands represent di-, mono-, and un-glycosylated isoforms at approximately 32, 23 and 18 kDa, respectively. (B) The values under –PK and +PK represent the percentage of the level of total amount of PrP (–PK) and of PrP<sup>Sc</sup> (+PK) normalized to the control (100%). Values are the means  $\pm$  SD calculated from the four independent experiments performed.

## 3.2.2 Prion inhibition of 1 on ScN2a cells

The promising activity of 1 at 1  $\mu$ M was confirmed employing 8-point dose-response curves ranging from 0 to 4  $\mu$ M. In parallel, we assessed cell viability at different concentrations of 1 (up to 10  $\mu$ M) and its non-toxic profile was confirmed (Table S4).

The IC<sub>50</sub> was calculated using an ELISA assay of PK digested samples from ScN2a-RML cells and confirmed by Western blotting analysis. We measured an IC<sub>50</sub> (calculated with IGOR software) of  $0.42 \pm 0.1 \,\mu\text{M}$  (Figure 5).



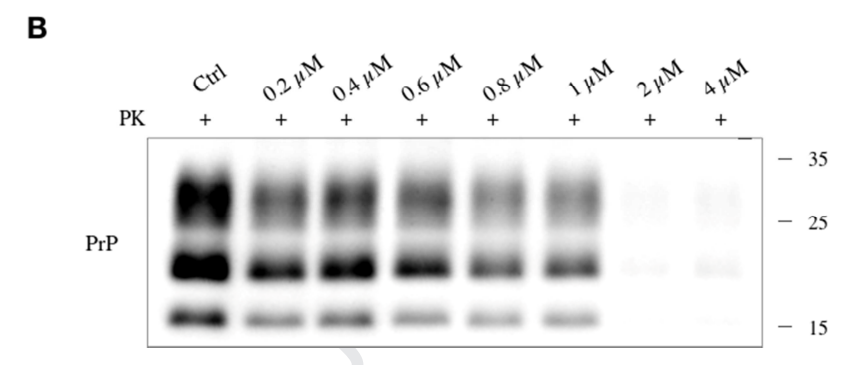


**Figure 5.** IC<sub>50</sub> determination of 1 on ScN2a-RML. (A) Dose-response curve form ELISA assay of 8 different concentrations of 1. (B) Western blot of ScN2a-RML cell lysates treated with 1 at the same concentrations used in (A), after digestion with proteinase K.

As 1 showed a very promising profile in terms of safety and dose-dependent activity, the next step was to resynthesize 1, with the aim of validating the biological activity of the vendor-supplied sample, and in order of obtaining a sufficient amount to perform further studies.

Particularly, as no synthetic protocol was reported, we aimed to develop a versatile synthetic procedure that would also allow further chemical manipulation, starting from easily accessible building blocks.

Thus, the synthesis of **1** was achieved through a simple two-step reaction, depicted in Scheme 1. Hydrazine **16**, was synthesized through a solvent-free, nucleophilic substitution of 4,7-dichloroquinoline by hydrazine using microwave irradiation [40]. Then, **16** (1 eq) was condensed

with 2-acetylphenothiazine in acetic acid and ethanol, affording **1** in a good yield (81%). **1** identity was confirmed by analytical (HPLC), full scan MS (ESI+) and spectroscopic data (<sup>1</sup>H-NMR), which were identical to those of the commercial sample.

4,7-dichloroquinoline

$$\downarrow a$$

$$\downarrow NHNH_2$$

$$\downarrow Cl$$

$$\downarrow Cl$$

$$\downarrow A$$

**Scheme 1.** Synthetic procedure for the synthesis of **1**. Reagents and conditions: a) NH<sub>2</sub>NH<sub>2</sub>, 5 min, 150°C, MWI; b) EtOH, AcOH, 24h, reflux.

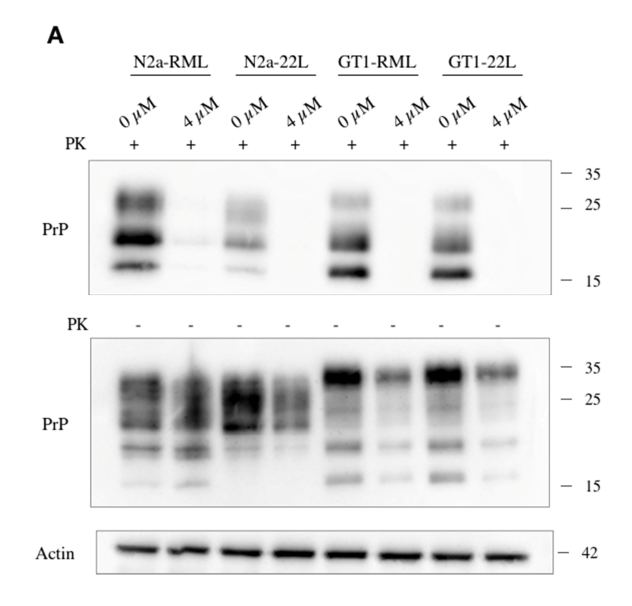
## 3.2.3 Prion inhibition of 1 on different cell lines and prion strains

It is known from the literature that several small molecules are active only on precise cell lines and on some prion strains and not on others, these phenomena are called cell and strain specificity [41–43]. The strain specificity occurs with molecules that exert their interaction by either directly binding to  $PrP^{Sc}$  or both  $PrP^{C}$  and  $PrP^{Sc}$ , since the strain specificity seems to derive from the alternate folding of  $PrP^{Sc}$  [44]. Therefore, we decided to test 1 on three other cell lines: ScN2a chronically infected with 22L mouse prion strain, ScGT1 infected with two prion strains, RML and 22L.

In Figure 6A, the Western blots of cell lysates are shown. In accordance with the previous results, 1 resulted to be not toxic at 4  $\mu$ M on these cells (data not shown)).

On ScN2a-RML 1 reduces the level of PrP<sup>Sc</sup> to about 10%, showing a strong clearance of PrP<sup>Sc</sup>. This activity is maintained in the other cell lines (5% for N2a-22L and 10% for GT1-RML and GT1 22L) (Figure 6B). The total amount of PrP (samples non-treated with proteinase K) also seems to be reduced in all the cell lines. This reduction is probably due to the clearance of PrP<sup>Sc</sup> visible in the PK-treated samples.

Controls are normalized to 100% of untreated PK-digested samples (upper square in Figure 6A) the amount of PrP<sup>Sc</sup> may not result the same and this reflects the difference in PrP<sup>Sc</sup> protein level in different cell lines.



В

Cell line	Concentration (µM)	–PK	+PK
ScN2a-RML	0	100.0	100.00
SCINZA-KIVIL	4	$62.1 \pm 3.4$	$9.4 \pm 2.8$
ScN2a-22L	0	100.0	100.0
SCINZA-ZZL	4	$48.7 \pm 12.4$	$5.1 \pm 4.5$
ScGT1-RML	0	100.0	100.0
	4	$42.0 \pm 3.8$	$12.3 \pm 5.3$
ScGT1-22L	0	100.0	100.0
	4	$39.2 \pm 9.6$	$11.0 \pm 8.0$

Figure 6. Activity of 1 on the total PrP or PrP<sup>Sc</sup> on ScN2a-22L, ScGT1-RML, ScGT1-22L. (A) One of the three WBs carried out using the cell lysates of treated and untreated cells with 1, before and after PK digestion. (B) Quantification of the three independent experiments performed. The values under -PK and +PK point the percentage of the level of the total amount of PrP (-PK) and of PrP<sup>Sc</sup> (+PK) normalized to the control (100 %). Values are the means  $\pm$  SD calculated from the four independent experiments performed.

## 3.3 Understanding the mechanism of action of 1

Small molecules can block prion replication through three main strategies: (i) by directly blocking prion replication (via PrP<sup>C</sup> stabilization or PrP<sup>Sc</sup> destabilization); (ii) by modulating other proteins involved in the prion replication; (iii) by increasing PrP<sup>Sc</sup> clearance/degradation.

We therefore attempted to elucidate the mechanism responsible of the strong reduction of prions by 1.

## 3.3.1 Compound 1 does not affect the PrP<sup>C</sup> localization from the cell membrane

Antipsychotic drug chlorpromazine (CPZ) has been shown to inhibit prion replication by directly binding to  $PrP^{C}$  [45]. However, biophysical studies have revealed that its affinity to  $PrP^{C}$  is in a high micromolar range ( $K_{D}$ =421  $\mu$ M), while the active concentration on infected cells is 100 times lower. Knowing that the antipsychotic effect of CPZ involves the clathrin-mediated endocytosis (CME) and that CME allows the recycling of  $PrP^{C}$  from the plasma membrane, a recent study shown that CPZ promotes relocalization of  $PrP^{C}$  from the cell surface to the intracellular compartments [14].

CPZ and 1 are both phenothiazine derivatives. So, based on the similar chemical structure, the following experiments were conducted to test if the mechanism of action of 1 involves a redistribution of PrP<sup>C</sup>.

An immunofluorescence surface staining was performed using N2a cells treated with compound 1 at two different concentrations: 0.4 and 4  $\mu$ M. We expected that if 1 can promote a re-localization of PrP<sup>C</sup> as in the case of CPZ treatment (Figure S3), the samples treated with the molecule at 0.4  $\mu$ M, but especially at 4  $\mu$ M, should exhibit a decrease in the level of PrP<sup>C</sup> stained in respect to the untreated and the mock controls. On the contrary, we noticed that treated samples had the same staining pattern of controls (Figure 7).

We concluded that anti-prion effect of **1** does not involve a PrP<sup>C</sup> redistribution from the cell surface to the intracellular compartments, as is the case for CPZ and other phenothiazine derivatives.

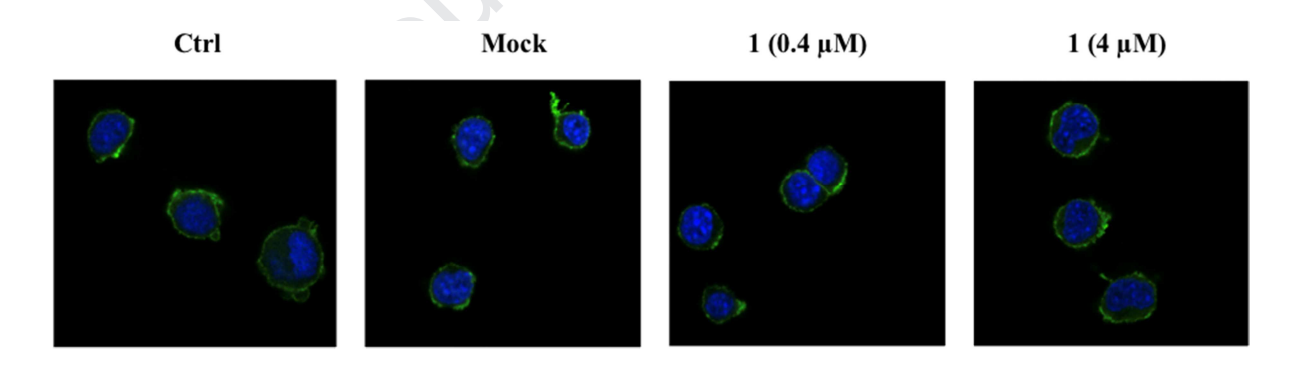


Figure 7. Surface immunofluorescent staining on N2a cells treated with 1. Two different concentration of 1 were used:  $0.4 \mu M$  and  $4 \mu M$ .  $PrP^{C}$  present on the surface is labeled in green, and in blue the nucleus.

## 3.3.2 Activity of 1 in the in vitro prion conversion

 ${f 1}$  does not affect the levels of the cellular PrP (data not shown) and the treatment of uninfected N2a cells does not disturb redistribution of the PrP<sup>C</sup> from the plasma membrane to intracellular compartments.

In order to elucidate mechanism of action of 1, we checked whether it is actually able to bind the  $PrP^{C}$ .

We used the SPR to check a hypothetical binding between  $\mathbf{1}$  and the  $PrP^{C}$  and eventually calculate the dissociation constant ( $K_{D}$ ). Unfortunately, due to interference with EtOH/DMSO solution in which  $\mathbf{1}$  was dissolved, this technique was inconclusive. For this reason, we tried to avoid the use of SPR and we designed a new protocol to evaluate the possible binding between  $\mathbf{1}$  and  $PrP^{C}$ , that we named competition assay (see Materials and Methods section and Figure S1).

In this assay, PrP and 1 were mixed in different ratios and incubated with constant shaking for 30 minutes. Then the mix and 1 alone were centrifuged in Nanosep centrifugal device with a 3 kDa membrane to pass the whole solution through. These tubes are permeable for 1 (416.93 Da) but not for the PrP (25 kDa) and the hypothetical PrP-1 complex.

All the solutions were then analyzed using two different approaches: with WB where they were added to the N2a-RML cells and in the RT-QuIC where they were loaded into a 96-well plate. If the binding between PrP and 1 would occur, a decrease of PK-resistant PrP<sup>Sc</sup> in the WB and inhibition of the prion aggregation in RT-QuIC are expected.

## 3.3.2.1 Competition assay on ScN2a cells

Then, the solution from the bottom of the tube after the centrifugation was added to the ScN2a cells as a normal treatment for 4 days.

As a negative control, we used cells treated just with the vehicle. The cells incubated with 1  $\mu$ M of 1 without the centrifugation in the Nanosep centrifugal device and the ScN2a treated with 1  $\mu$ M of 1 after the use of Nanosep tubes were utilized as positive controls.

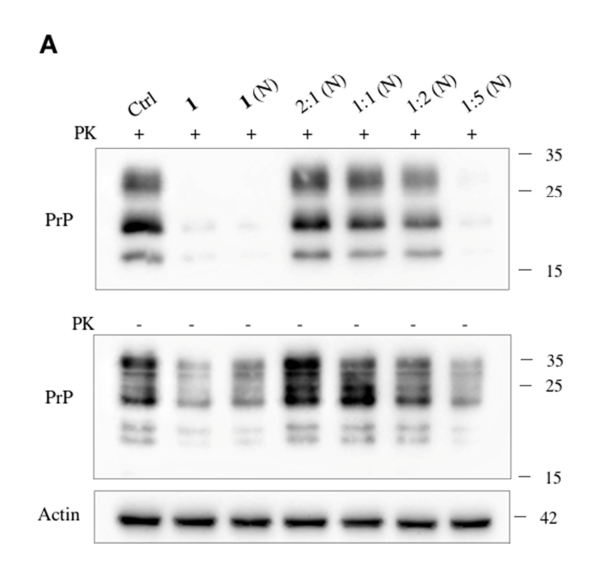
From the WB analysis (Figure 8A), we noticed that the treatment with 1 without the use of Nanosep tube and the treatment with the solution obtained after putting 1 alone in the tube caused the same effect on the ScN2a. In both cases, it is possible to see a strong and a very similar reduction of the PrPSc. This result confirmed the functionality of the Nanosep device, because it means that 1 alone is able to cross the membrane, indeed 3kDa > 416.93Da (1 MW). Once we concluded this, we checked what happened when the PrP and 1 are put in the Nanosep tubes after a pre-incubation at 37 °C with shaking. As it is possible to see in Figure 8A, when the ratio is 2 moles of PrP and 1 mole of 1 or 1 mole of PrP and 1 of 1, the level of PK-resistant PrPSc is not affected by a strong reduction as it happened after the addition of 1 alone.

This means that when the two molecules are incubated in the ratios 2:1 and 1:1, there is a binding between 1 and PrP that does not allow the 1 to cross the membrane, otherwise the results would have the same pattern of those in line 1 and 1 (N), since the 1 crosses the 3kDa membrane of the

Nanosep tubes. After the quantification, this result is even more evident. Treatment directly with 1 or after the use of Nanosep device produced a PrP<sup>Sc</sup> inhibition around 30%, while in the 2:1(N) and 1:1(N) did not cause any or a strong inhibition, the values are around 100% and 90% (Figure 8B). When the mixes were prepared in a ratio 1:2, 1 mole of PrP and 2 moles of 1, the level of resistant-PK PrP<sup>Sc</sup> decrease to 65%, demonstrating that a part of 1 was linked to the PrP and the other crossed the Nanosep membrane and affected the level of PrP<sup>Sc</sup>. We also used a ratio in which the concentration of 1 is 5 times higher than the PrP (1:5). The strong inhibition of PrP<sup>Sc</sup> from 100% to 23.6%, using the ratio 1:5, could be explained again through the binding between PrP and 1. In this case the level of PrP<sup>Sc</sup> is the same as in the samples treated just with 1, probably because 1 is in a large excess causing the majority of it to cross the 3 kDa membrane.

All the results obtained using the different ratios and treating the cells with the solution present in the Nanosep device's bottom, led us to believe that the 1 is actually able to bind the PrP.

The level of total PrP followed the same trend of PrP<sup>Sc</sup>, even if the decrease is less evident. This shows that **1** is able to affect just the PrP<sup>Sc</sup> level, although it binds the PrP<sup>C</sup>.



B

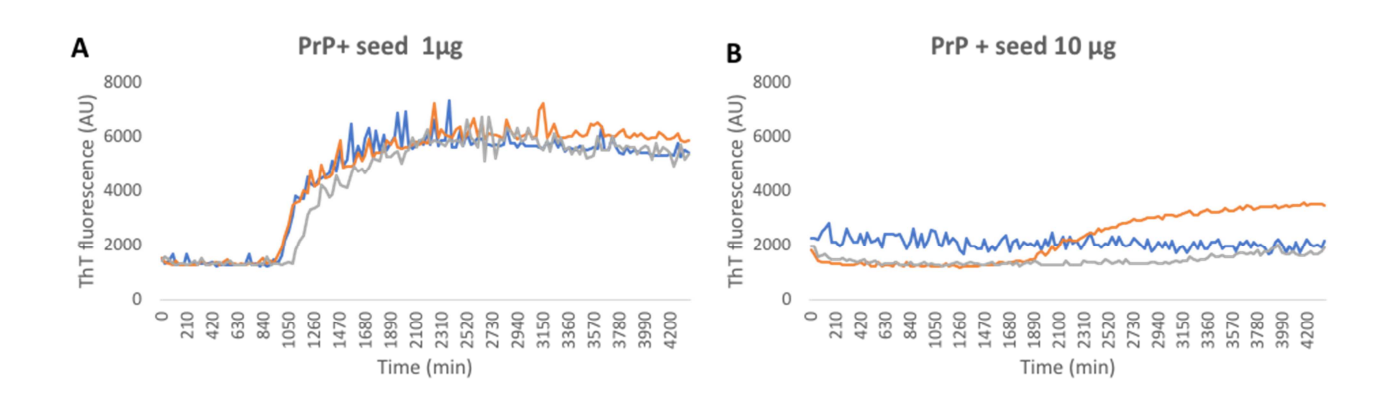
Condition	–PK	+PK
Ctrl	100	100
1	$48.8 \pm 4.5$	$25.2 \pm 7.8$
1 (N)	$51.7 \pm 6.7$	$22.6 \pm 9.5$
2:1 (N)	114.4 ± 7.1	$108.2 \pm 3.8$
1:1 (N)	$117.6 \pm 7.3$	90.1 ± 2.9
1:2 (N)	$98.4 \pm 5.2$	$65.7 \pm 5.7$
1:5 (N)	$41.0 \pm 4.8$	$13.6 \pm 9.0$

Figure 8. Competition assay in ScN2a cell line. (A) Representative WB of the cell lysates of ScN2a treated with the different conditions. The first line corresponds to the untreated sample, then in order: sample incubated with 1  $\mu$ M of 1, samples treated with the solution obtained from the bottom part of Nanosep device after centrifugations of 1 alone, cells incubated with the solution obtained from the bottom part of Nanosep device after centrifugations of a pre-incubated PrP and 1 in ratios 2:1, 1:1, 1:2 and 1:5. In the upper part the cell lysates are represented after the PK-digestion (PrPSc), in the bottom the samples without the PK treatment. (B) The table shows the quantification of the three-independent experiment performed. The values under –PK represent the normalization of the total PrP on the actin, the values under +PK represent the PrPSc on the total PrP. Values are the means  $\pm$  SD calculated from the three independent experiments performed.

## 3.3.2.2 Competition assay using RT-QuIC

To confirm our results, we decided to perform RTQuIC analysis. WB and RTQuIC are different techniques, with advantages and disadvantages. In the WBs it is possible to see the effect of the treatment on living cells, but it is possible to detect only the presence of PK-resistant PrP<sup>Sc</sup> and only if there is enough amount of protein. On the other side, with the RTQuIC technique it is not possible to consider all the other potential factors that are present in cells and that can trigger the spreading of PrP<sup>Sc</sup>, however, it is able to detect very low amounts of prions.

In the RT-QuIC assay, the MoPrP (23-231) alone was used as a negative control, because it is known that this protein is not able to aggregate in the absence of a seed [46]. Instead, the positive control consists of PrP with a  $PrP^{Sc}$  seed. We tested two different amounts, 1  $\mu g$  and 10  $\mu g$ , and tested which one gave the best result in terms of seeding activity and reproducibility. Figure 9 A and B show the curves using the two different seeds.



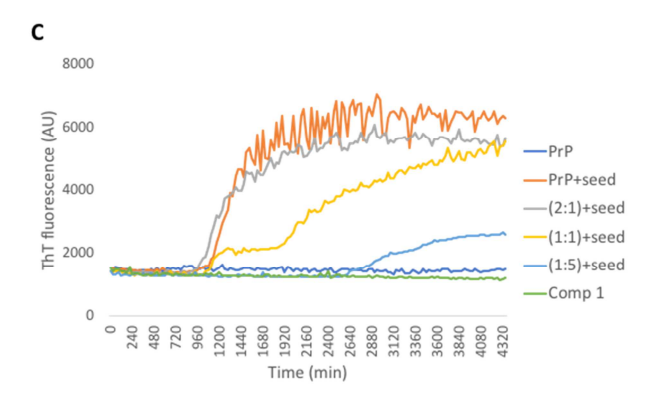


Figure 9. Aggregation curves of MoPrP (23-231) using 1  $\mu g$  or 10  $\mu g$  of the seed and after the treatments with the solution obtained with the competition assay. Three independent RT-QuIC experiments, each one represented by a specific color. (A) The aggregation is promoted by 1  $\mu g$  of the seed. (B) The aggregation of PrP is allowed by 10  $\mu g$  of the seed. (C) The dark blue line is the PrP alone, the orange is the PrP with the seed, in gray the aggregation curve of the PrP after the addition of the solution obtained after the pre-incubation and centrifugation in the Nanosep device of the mix consisting PrP and 1 in a ratio 2:1, in yellow 1:1 and in light blue 1:5, in green the 1 alone at 1  $\mu$ M. Each curve represents the average of three independent experiments.

Using only the seed at 1  $\mu$ g, we obtained an aggregation curve, for this reason we decided to use 1  $\mu$ g of seed for the later experiments.

We have set up an RT-QuIC protocol, by which the negative control consists of only PrP, that did not show a curve aggregation and the positive control which it has a reproducible curve aggregation after about 1050 min (17,5 hours) (Figure 10C).

As before, the same competition assay procedure was performed, but instead of cell treatment, the solutions were added to the 96 well plate.

The experiments confirmed what we saw in the WBs, the solution obtained from the pre-incubation of PrP:1=2:1 after several centrifugations using the Nanosep device contains prions. Indeed, it is possible to observe that the aggregation curves have the same ThT fluorescence, around 6000 AU, and the lag phase (1050 min) as the positive control. Also, in the WBs analysis, the level of PrP<sup>Sc</sup> in this condition was the same of the untreated control. So, these two different assays support our hypothesis that 1 binds PrP and so it is not able to cross the 3kDa membrane present on the Nanosep device and to inhibit PrP<sup>Sc</sup> and its aggregation. When the ratio used is PrP: 1=1:1, the aggregation curves of the three independent experiments are not comparable. Also, in this case the RT-QuIC assay confirmed the WBs results. The increase of the lag phase and the decrease of ThT fluorescence can mean a lower presence of prions and this could correspond to the results of the WB, where after the treatment with the solution obtained from PrP: 1=1:1 mix, the level of PrP<sup>Sc</sup> started to decrease. These results mean that at the ratio 1:1, almost all molecules of 1 bind the PrP, causing just a small inhibition of prions aggregation. In Figure 9C, results from the RT-QuIC of PrP

treated with the solution obtained after the pre-incubation and centrifugation in the Nanosep tubes of the mix PrP:1 = 1:5 is also represented. The delayed aggregation curves (starting around 50 hours) and the low ThT fluorescence (4000 AU) could be due to a low presence of prions, that corresponds exactly to the strong inhibition of the PK-resistant PrP<sup>Sc</sup> seen in WB. This again could mean that even if 1 binds PrP it is in a large excess and can cross the 3kDa membrane. So, when the solution in the bottom of the Nanosep tube is added to the 96-well plate, there is enough of 1, which is able to bind the PrP<sup>C</sup> and partially inhibit the aggregation.

Control experiments were also performed, in order to confirm that the vehicle (EtOH-DMSO) does not influence the results (Figure S2).

Taking together the WBs and RT-QuIC experiments, we conclude that the **1** is able to bind the PrP (23-231) and so the cellular prion protein.

## 3.3 Effect of chronic treatment with 1 on ScN2a cell line

A possible cause of the common clinical failure of several small molecules that had been previously shown to decrease the level of mouse PrP<sup>Sc</sup> and/or inhibit the prion aggregation [30,47–50] is the drug-prion resistance developed after a continuous chronic treatment and the prion strain selection. This is what happened for quinacrine treatment in prion-inoculated MDR<sup>0/0</sup> mice [51].

In order to assess if ScN2a-RML cells treated with 1 can be walking into a strain resistant and to check if the therapeutic potential of 1, a chronic treatment was performed. We treated ScN2a-RML cells with 4  $\mu$ M of 1 for 5 passages that correspond to 20 days of treatment. After this period, the incubation with 1 was stopped and the cells were maintained in culture without any treatment for other 5 passages to check if this kind of treatment with 1 for 20 days is able to clear completely cells from prions (Figure 10A).

After 40 days, 10 passages of ScN2a-RML cells were obtained. This experiment was performed 3 times and each time in double, because we assessed the activity of **1** in chronic treatment using both WB analysis and RT-QuIC assay.

For the WBs, we used the lysates of uninfected N2a cells and the ScN2a-RML before the treatment (#0) as controls. So, looking at the WB, it is possible to notice that the  $PrP^{Sc}$  in N2a cells is absent, as expected. Indeed, after PK-digestion no signal was detected. At #0, ScN2a-RML cells showed the typical pattern of the RML prion strains: the three bands with the mono-glycosylated one more evident. But immediately after the first passage of the 4  $\mu$ M treatments with 1, PK-resistant  $PrP^{Sc}$  is almost absent. In the following passages (from #2 to #10) the  $PrP^{Sc}$  is not even detectable. It is very important to focus the attention on the fact that from the #6 to #10 the treatment with 4  $\mu$ M of 1 is stopped. So, the absence of  $PrP^{Sc}$  signal in these passages shows that the 1 is able to "cure" the

ScN2a-RML cells from prions and that it does not undergo a drug-prion resistance. The level of total PrP was evaluated, observing the samples not treated with PK-digestion. The total PrP does not reflect the results obtained for the PrP<sup>Sc</sup>, because in this case the #0 and #1 have the exactly same pattern, while in the PK-treated samples the level of PrP was strongly reduced already in the #1. Conversely, the total PrP signal from #2 until #10 is unchanged, but is exactly the same of the PrP<sup>C</sup> signal from the uninfected N2a cells (line 1). Thus, from the WB it seems that in the samples of ScN2a-RML since the #2 the only prion protein present is the cellular prion protein.

The same samples were checked also in the RT-QuIC assay. After cell collection, the pellet was dissolved in 50  $\mu$ l of PBS and then sonicated. The sonicated proteins were quantified, as already mentioned in the previous paragraph, and 1  $\mu$ g of them was used as seed. In Figure 10C, it is possible to observe the RT-QuIC experiments that we performed with the same type of samples used for WBs, to compare the two different approaches. In the control (Figure 10C, orange line), without treatment with 4  $\mu$ M of 1, prion aggregation started after 1050 minutes (17,5 hours). The same result was obtained in the #1, where the ThT fluorescence intensity and the lag phase were identical as in #0. At #1 the aggregation curve obtained in RT-QuIC (Figure 10C, gray line) reflects the WB result without the digestion with the proteinase K (Figure 10B), but not the result of the PK-digested sample.

While in WB, at #2, in both PK and non-PK treated samples, the PrPSc seemed completely cleared, in RT-QuIC experiments, the lag phase was a little elongated (1260 minutes, 21 hours) and the ThT fluorescence was decreased, for some peaks to 7000 AU in #0 and #1 to 5000 AU in #2 (Figure 10C, yellow line). The same kind of incongruence was noticed in #3, because in the WB the PrPSc signal is completely absent, while in the RT-QuIC the presence of prions is evident by the aggregation curve (Figure 10C, light blue line). At passage #4, in two out of three experiments, the PrP is not able to aggregate; just one sample started the aggregation around 45 hours (2730 minutes) (Figure 10C, light green line). We did not consider it as a technical problem, because all the 4 wells of that experiment aggregate at the same time and with the same intensity, rather we believed that after 4 passages of treatment with 1, the prions in almost all the experiments were cleared but it is possible that sometimes they were not completely eliminated. Importantly, the fifth treatment with 1 is incontrovertibly able to remove all the prions present in the ScN2a-RML cells and the proof is the absence of an aggregation curve in all the passages after the #5.

The fact that even after the #5 that corresponds to the treatment interruption none of the samples demonstrated to have prions using both the RT-QuIC assay and WB analysis, confirmed the ability of 1 at  $4 \mu M$  of concentration to cure the ScN2a from the RML prion strain.

Looking at the results, this reduction is mainly characterized with a decrease in the ThT fluorescence, rather than in an increase in the lag phase.

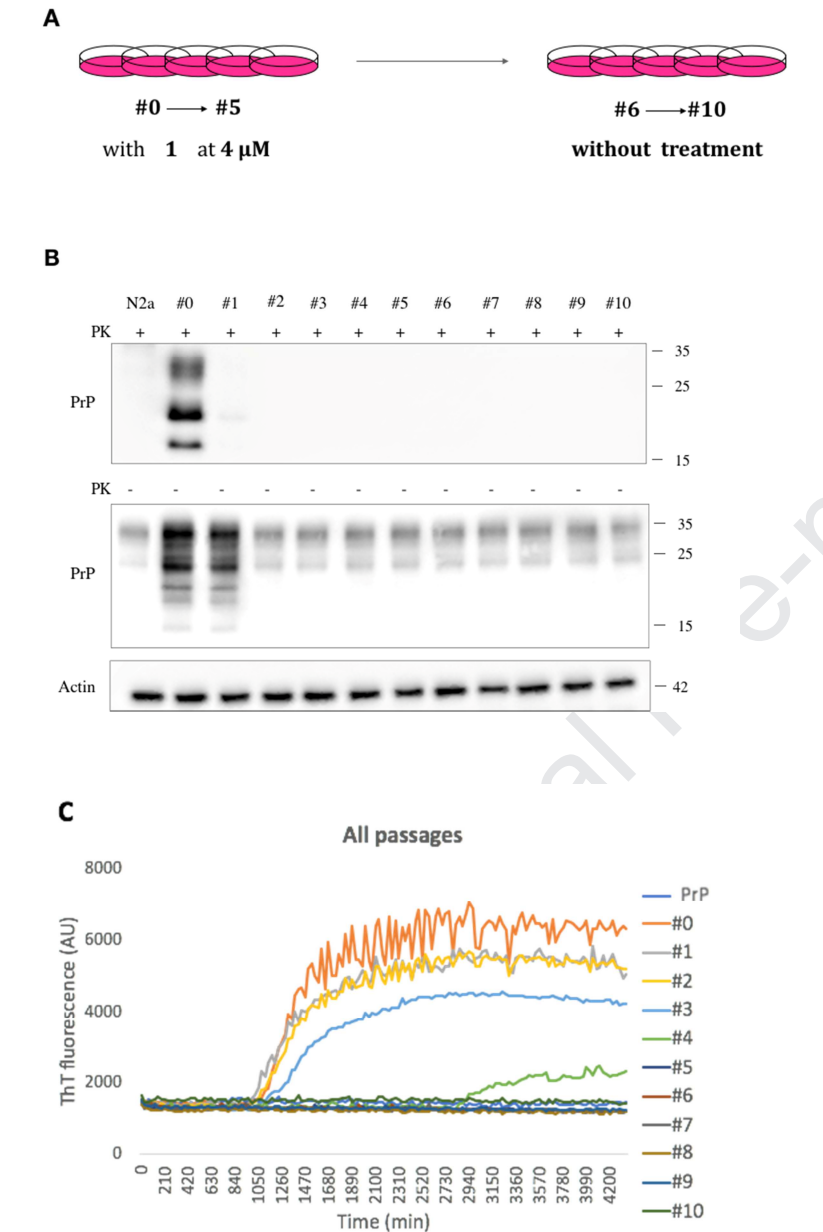


Figure 10. Chronic treatment with 1 on ScN2a-RML cells. (A) Schematic representation of the chronic treatment with 1. ScN2a-RML cells were incubated with 4  $\mu$ M of compound 1 for 5 passages, after this period the treatment was stopped, and the cells were passaged for others 5 times. (B) Representative WB of ScN2a-RML cell lysates. The upper part corresponds to the PK-resistant PrP<sup>Sc</sup> detected using the W226 primary antibody. The same was used in the cell lysates not subjected to PK-digestion. In the bottom part the actin is represented, detected using the anti β-actin antibody. (C) Aggregation curves of PrP after the addition of a seed, obtained from a chronic treatment on ScN2a-RML cells. RT-QuIC performed with 0.2 mg of PrP and using 1  $\mu$ g of sonicated protein from ScN2a-RML cells. The RT-QuIC experiment using only the PrP is shown in blue. As it is presented in the legend the different colors represented curve aggregation using as a seed the different passages obtained from the N2a-RML treated with 1.

## 3.4 Design and synthesis of more soluble 1 analogues

Despite its low effective concentration ( $IC_{50}$ ) in vitro, advancement of **1** as a promising lead candidate was limited by a low solubility (see below), which might negatively affect its absorption, and makes difficult to perform further in vivo studies. In light of this, we decided to improve **1**'solubility by functionalizing the nitrogen of the phenothiazine ring, through the insertion of polar groups. Derivatives **11-15** (Figure 11), bearing dimethylamino, piperidino, morpholino and methylpiperazino groups linked to the phenothiazine ring by spacers of 2/3 methylenes, were synthesized. Importantly, the selected solubilizing groups were carefully selected among those more frequently employed for the design and optimization of CNS drugs [52].

Figure 11. Chemical structures of 1 derivatives 11-15.

We performed the planned structural modifications using the synthetic sequence described in Scheme 2.

**Scheme 2. Synthetic procedure for the synthesis of derivatives 11-15**. Reagents and conditions: a) NaH, DMF, 5h, 50°C; b) **16**, EtOH, AcOH, 24h, reflux.

The N-substituted 2-acetylphenothiazine-derivatives **17-21** were synthesized through a simple N-alkylation of 2-acetylphenothiazine with the corresponding Cl-derivatives **22-26** (Scheme 2). In

details, 2-acetylphenothiazine (1 eq) was reacted with **22-26** (2 eq), in the presence of NaH in DMF, affording **17-21** with low to good yields.

The aqueous solubility of all compounds at pH 7.4 was determined as shown in Table S5. The introduction of the solubilizing groups led to significantly improved solubilities compared to the unsubstitued parent 1. Particularly, alkyldimethhylamino derivatives 11 and 12 were the most soluble of the series, being about 30 and 50 times more soluble than 1.

Then, the newly synthesized compounds were subjected to cell-based assays to ascertain their antiprion activity. Compounds were tested at 1  $\mu$ M concentration, and dimethylamino (11 and 12), piperidino (13), and methylpiperazino (15) derivatives were even able to improve the ability of the parent compound 1 to reduce  $PrP^{Sc}$ , with and without treatment with PK. The morpholino derivative 14 was the less potent of the series, while the methylpiperazino 15 the most active one (4.4 and 55.9% reduction, respectively) (Figure 12).

Compound	+PK (%)	-PK (%)
Ctrl	100	100
1	$35.2 \pm 8.8$	$60.4 \pm 6.3$
11	$8.6 \pm 0.2$	$60.2 \pm 5.7$
12	$11.9 \pm 3.4$	$68.7 \pm 3.2$
13	$13.6 \pm 1.2$	$70.2 \pm 7.5$
14	$70.3 \pm 6.3$	$95.3 \pm 6.2$
15	$4.4 \pm 2.1$	$55.9 \pm 2.8$

Figure 12. Anti-prion effect evaluation of 1's derivatives 11-15 at 1  $\mu$ M of concentration. The table shows the WB quantification of the three-independent experiment performed. The values under –PK represent the normalization of the total PrP on the actin, the values under +PK represent the PrP<sup>Sc</sup> on the total PrP. Values are the means  $\pm$  SD from three independent experiment.

#### **Conclusions**

Prion diseases are triggered by the accumulation of aberrant misfolded isoforms of PrP<sup>C</sup> in the central nervous system (CNS). The conformational change and replication of the PrP<sup>C</sup> into its pathological isoform PrP<sup>Sc</sup> are followed by aggregation and cell spreading in the CNS, which lead to fatal neurodegeneration. So far, no therapies against TSEs have been identified. A number of molecules have been developed and many have been tested in human clinical trials with no positive

results [18,22,24,26,53,54], highlighting the challenging task of developing anti-prion drugs and consequently understanding their mechanism of action.

In this study, a QSAR model has been developed to identify new chemotypes through virtual library screening. 1 emerged as the most promising molecule, so attempts were made to assess its mechanism of action.

The efficient profile of **1** might be ascribed to the bivalent structure of this molecule, which consists of two main moieties, i.e. a phenothiazine and a 7-chloro-quinoline, bound by a hydrazone linker (Figure 11). The two moieties are very well-known prion recognition motifs. The phenothiazine moiety was reported to be an anti-prion agent in ScN2a-RML [55]. Likewise, several quinoline derivatives, containing 7-chloro-quinoline fragment, have been tested as potential anti-prion drugs with excellent results [56].

So, we conclude that the strong efficacy of **1** to inhibit prion formation and to reduce PrP<sup>Sc</sup> from prion infected cells is linked to its bivalent structure consisting of two pharmacophores separated by a linker [64, 65]. No one of the other selected molecules (2-10) share these peculiar chemical features.

The three main cellular effects of anti-prion small molecules are: (i) PrP<sup>C</sup> stabilization; (ii) the modulation of other proteins involved in the replication process and (iii) the increase of PrP<sup>Sc</sup> clearance. We design a competition assay protocol to evaluate a possible binding between 1 and PrP. The results have shown the ability of 1 to bind the PrP (23-231).

As our work progressed, low solubility of 1 was observed as a major liability for further development. Therefore, we have sought to overcome this challenge by generating more soluble compounds. Particularly, we applied the efficient route developed for the synthesis of 1 to the synthesis of five derivatives, purposely designed to overcome its low solubility liability. Thus, by slightly modifying its structure, five derivatives that bear classical solubilizing groups were developed. Solubility assay confirmed our design strategy, as we were able to increase solubility from 3 to 50 times. More importantly, we verified how the performed modification affected the activity. Notably, the introduction of an alkylamino chain on the phenothiazine ring makes that portion of the molecules highly resemblance of phenothiazine antipsychotics, which have been clinically used for decades and widely shown to possess anti-prion activity. In addition, a phenothiazine moiety connected to an amino functionality through an alkyl linker has been recognized as a privileged neuroprotective structure for the development of new small molecules against neurodegenerative diseases [57]. Both these issues seem positive in terms of further developability of this series of molecules.

In this respect, one potential problem with **1** and more soluble derivatives is the presence of the labile hydrazide linker, which might produce *in vivo* toxic aryl hydrazine metabolites. Medicinal chemistry studies are ongoing to replace the hydrazide functionality and to expand the utility of this promising hit compounds as lead candidates against prion diseases.

## References

- [1] F.U. Hartl, Protein Misfolding Diseases, Annu. Rev. Biochem. 86 (2017) 21–26. https://doi.org/10.1146/annurev-biochem-061516-044518.
- [2] L.C. Walker, H. LeVine, The cerebral proteopathies, Neurobiol. Aging. 21 (2000) 559–561. https://doi.org/10.1016/S0197-4580(00)00160-3.
- [3] S.B. Prusiner, Cell biology. A unifying role for prions in neurodegenerative diseases, Science. 336 (2012) 1511–1513. https://doi.org/10.1126/science.1222951.
- [4] M.L. Bolognesi, G. Legname, Approaches for discovering anti-prion compounds: lessons learned and challenges ahead, Expert Opin. Drug Discov. 10 (2015) 389–397. https://doi.org/10.1517/17460441.2015.1016498.
- [5] S. Aulić, T.T.N. Le, F. Moda, S. Abounit, S. Corvaglia, L. Casalis, S. Gustincich, C. Zurzolo, F. Tagliavini, G. Legname, Defined α-synuclein prion-like molecular assemblies spreading in cell culture, BMC Neurosci. 15 (2014) 69. https://doi.org/10.1186/1471-2202-15-69.
- [6] F. Clavaguera, T. Bolmont, R.A. Crowther, D. Abramowski, S. Frank, A. Probst, G. Fraser, A.K. Stalder, M. Beibel, M. Staufenbiel, M. Jucker, M. Goedert, M. Tolnay, Transmission and spreading of tauopathy in transgenic mouse brain, Nat. Cell Biol. 11 (2009) 909–913. https://doi.org/10.1038/ncb1901.
- [7] C. Soto, In Vivo Spreading of Tau Pathology, Neuron. 73 (2012) 621–623. https://doi.org/10.1016/j.neuron.2012.02.006.
- [8] A. Ulusoy, R.E. Musgrove, R. Rusconi, M. Klinkenberg, M. Helwig, A. Schneider, D.A. Di Monte, Neuron-to-neuron α-synuclein propagation in vivo is independent of neuronal injury, Acta Neuropathol. Commun. 3 (2015) 13–13. https://doi.org/10.1186/s40478-015-0198-y.
- [9] D.L. Ritchie, J.W. Ironside, Chapter Fourteen Neuropathology of Human Prion Diseases, in: G. Legname, S. Vanni (Eds.), Prog. Mol. Biol. Transl. Sci., Academic Press, 2017: pp. 319–339. https://doi.org/10.1016/bs.pmbts.2017.06.011.
- [10] A. Kraus, B.R. Groveman, B. Caughey, Prions and the potential transmissibility of protein misfolding diseases, Annu. Rev. Microbiol. 67 (2013) 543–564. https://doi.org/10.1146/annurev-micro-092412-155735.
- [11] S.B. Prusiner, Prions, Proc. Natl. Acad. Sci. U. S. A. 95 (1998) 13363–13383. https://doi.org/10.1073/pnas.95.23.13363.
- [12] H.M. Schätzl, M.D. Costa, L. Taylor, F.E. Cohen, S.B. Prusiner, Prion Protein Gene Variation Among Primates, J. Mol. Biol. 245 (1995) 362–374. https://doi.org/10.1006/jmbi.1994.0030.
- [13] D. Riesner, Biochemistry and structure of PrPC and PrPSc, Br. Med. Bull. 66 (2003) 21–33. https://doi.org/10.1093/bmb/66.1.21.
- [14] C. Stincardini, T. Massignan, S. Biggi, S.R. Elezgarai, V. Sangiovanni, I. Vanni, M. Pancher, V. Adami, J. Moreno, M. Stravalaci, G. Maietta, M. Gobbi, A. Negro, J.R. Requena, J. Castilla, R. Nonno, E. Biasini, An antipsychotic drug exerts anti-prion effects by altering the localization of the cellular prion protein, PloS One. 12 (2017) e0182589–e0182589. https://doi.org/10.1371/journal.pone.0182589.

- [15] D.R. Dee, A.N. Gupta, M. Anikovskiy, I. Sosova, E. Grandi, L. Rivera, A. Vincent, A.M. Brigley, N.O. Petersen, M.T. Woodside, Phthalocyanine tetrasulfonates bind to multiple sites on natively-folded prion protein, Biochim. Biophys. Acta BBA Proteins Proteomics. 1824 (2012) 826–832. https://doi.org/10.1016/j.bbapap.2012.03.011.
- [16] N.S. Pagadala, R. Perez-Pineiro, D.S. Wishart, J.A. Tuszynski, In silico studies and fluorescence binding assays of potential anti-prion compounds reveal an important binding site for prion inhibition from PrPC to PrPSc, Mol. Dyn. New Adv. Drug Discov. 91 (2015) 118–131. https://doi.org/10.1016/j.ejmech.2014.07.045.
- [17] ThomasW. Furlow, RichardJ. Whitley, FranzJ. Wilmes, REPEATED SUPPRESSION OF CREUTZFELDT-JAKOB DISEASE WITH VIDARABINE, Orig. Publ. Vol. 2 Issue 8297. 320 (1982) 564–565. https://doi.org/10.1016/S0140-6736(82)90652-3.
- [18] M.D. Geschwind, A.L. Kuo, K.S. Wong, A. Haman, G. Devereux, B.J. Raudabaugh, D.Y. Johnson, C.C. Torres-Chae, R. Finley, P. Garcia, J.N. Thai, H.Q. Cheng, J.M. Neuhaus, S.A. Forner, J.L. Duncan, K.L. Possin, S.J. Dearmond, S.B. Prusiner, B.L. Miller, Quinacrine treatment trial for sporadic Creutzfeldt-Jakob disease, Neurology. 81 (2013) 2015–2023. https://doi.org/10.1212/WNL.0b013e3182a9f3b4.
- [19] J. Collinge, M. Gorham, F. Hudson, A. Kennedy, G. Keogh, S. Pal, M. Rossor, P. Rudge, D. Siddique, M. Spyer, D. Thomas, S. Walker, T. Webb, S. Wroe, J. Darbyshire, Safety and efficacy of quinacrine in human prion disease (PRION-1 study): a patient-preference trial, Lancet Neurol. 8 (2009) 334–344. https://doi.org/10.1016/S1474-4422(09)70049-3.
- [20] C. Masullo, G. Macchi, Y.G. Xi, M. Pocchiari, Failure to Ameliorate Creutzfeldt-Jakob Disease with Amphotericin B Therapy, J. Infect. Dis. 165 (1992) 784–785. https://doi.org/10.1093/infdis/165.4.784.
- [21] J.F. Martínez-Lage, A. Rábano, J. Bermejo, M. Martínez Pérez, M.C. Guerrero, M.A. Contreras, A. Lunar, Creutzfeldt-Jakob disease acquired via a dural graft: failure of therapy with quinacrine and chlorpromazine, Surg. Neurol. 64 (2005) 542–545. https://doi.org/10.1016/j.surneu.2005.03.035.
- [22] N.V. Todd, J. Morrow, K. Doh-ura, S. Dealler, S. O'Hare, P. Farling, M. Duddy, N.G. Rainov, Cerebroventricular infusion of pentosan polysulphate in human variant Creutzfeldt–Jakob disease, J. Infect. 50 (2005) 394–396. https://doi.org/10.1016/j.jinf.2004.07.015.
- [23] I. Bone, L. Belton, A.S. Walker, J. Darbyshire, Intraventricular pentosan polysulphate in human prion diseases: an observational study in the UK, Eur. J. Neurol. 15 (2008) 458–464. https://doi.org/10.1111/j.1468-1331.2008.02108.x.
- [24] S. Haïk, G. Marcon, A. Mallet, M. Tettamanti, A. Welaratne, G. Giaccone, S. Azimi, V. Pietrini, J.-R. Fabreguettes, D. Imperiale, P. Cesaro, C. Buffa, C. Aucan, U. Lucca, L. Peckeu, S. Suardi, C. Tranchant, I. Zerr, C. Houillier, V. Redaelli, H. Vespignani, A. Campanella, F. Sellal, A. Krasnianski, D. Seilhean, U. Heinemann, F. Sedel, M. Canovi, M. Gobbi, G. Di Fede, J.-L. Laplanche, M. Pocchiari, M. Salmona, G. Forloni, J.-P. Brandel, F. Tagliavini, Doxycycline in Creutzfeldt-Jakob disease: a phase 2, randomised, double-blind, placebocontrolled trial, Lancet Neurol. 13 (2014) 150–158. https://doi.org/10.1016/S1474-4422(13)70307-7.
- [25] G. Forloni, M. Tettamanti, U. Lucca, Y. Albanese, E. Quaglio, R. Chiesa, A. Erbetta, F. Villani, V. Redaelli, F. Tagliavini, V. Artuso, I. Roiter, Preventive study in subjects at risk of fatal familial insomnia: Innovative approach to rare diseases, Prion. 9 (2015) 75–79. https://doi.org/10.1080/19336896.2015.1027857.
- [26] M. Otto, L. Cepek, P. Ratzka, S. Doehlinger, I. Boekhoff, J. Wiltfang, E. Irle, G. Pergande, B. Ellers-Lenz, O. Windl, H.A. Kretzschmar, S. Poser, H. Prange, Efficacy of flupirtine on cognitive function in patients with CJD, Neurology. 62 (2004) 714. https://doi.org/10.1212/01.WNL.0000113764.35026.EF.

- [27] A. Gallardo-Godoy, J. Gever, K.L. Fife, B.M. Silber, S.B. Prusiner, A.R. Renslo, 2-Aminothiazoles as therapeutic leads for prion diseases, J. Med. Chem. 54 (2011) 1010–1021. https://doi.org/10.1021/jm101250y.
- [28] T.R.K. Reddy, R. Mutter, W. Heal, K. Guo, V.J. Gillet, S. Pratt, B. Chen, Library Design, Synthesis, and Screening: Pyridine Dicarbonitriles as Potential Prion Disease Therapeutics, J. Med. Chem. 49 (2006) 607–615. https://doi.org/10.1021/jm050610f.
- [29] S. Bongarzone, M. Staderini, M.L. Bolognesi, Multitarget ligands and theranostics: sharpening the medicinal chemistry sword against prion diseases, Future Med. Chem. 6 (2014) 1017–1029. https://doi.org/10.4155/fmc.14.56.
- [30] L. Zaccagnini, S. Brogi, M. Brindisi, S. Gemma, G. Chemi, G. Legname, G. Campiani, S. Butini, Identification of novel fluorescent probes preventing PrPSc replication in prion diseases, Eur. J. Med. Chem. 127 (2017) 859–873. https://doi.org/10.1016/j.ejmech.2016.10.064.
- [31] A. Gandini, M.L. Bolognesi, Chapter Twenty Therapeutic Approaches to Prion Diseases, in: G. Legname, S. Vanni (Eds.), Prog. Mol. Biol. Transl. Sci., Academic Press, 2017: pp. 433–453. https://doi.org/10.1016/bs.pmbts.2017.06.013.
- [32] P. Gramatica, N. Chirico, E. Papa, S. Cassani, S. Kovarich, QSARINS: A new software for the development, analysis, and validation of QSAR MLR models, J. Comput. Chem. 34 (2013) 2121–2132. https://doi.org/10.1002/jcc.23361.
- [33] L. Zhou, L. Yang, S. Tilton, J. Wang, Development of a high throughput equilibrium solubility assay using miniaturized shake flask method in early drug discovery, J. Pharm. Sci. 96 (2007) 3052–3071. https://doi.org/10.1002/jps.20913.
- [34] C.A. Lipinski, F. Lombardo, B.W. Dominy, P.J. Feeney, Experimental and computational approaches to estimate solubility and permeability in drug discovery and development settings1PII of original article: S0169-409X(96)00423-1. The article was originally published in Advanced Drug Delivery Reviews 23 (1997) 3–25.1, Spec. Issue Dedic. Dr Eric Tomlinson Adv. Drug Deliv. Rev. Sel. Most Highly Cited Artic. 1991-1998. 46 (2001) 3–26. https://doi.org/10.1016/S0169-409X(00)00129-0.
- [35] C.W. Yap, PaDEL-descriptor: An open source software to calculate molecular descriptors and fingerprints, J. Comput. Chem. 32 (2011) 1466–1474. https://doi.org/10.1002/jcc.21707.
- [36] S. Pirhadi, F. Shiri, J.B. Ghasemi, Multivariate statistical analysis methods in QSAR, RSC Adv. 5 (2015) 104635–104665. https://doi.org/10.1039/C5RA10729F.
- [37] Translational Bioinformatics and Its Application, Springer, 2017., n.d.
- [38] Frontiers in Medicinal Chemistry, Volume (4), Bentham Science Publishers, 2010, n.d.
- [39] G. Poncet-Montange, S.J. St Martin, O.V. Bogatova, S.B. Prusiner, B.K. Shoichet, S. Ghaemmaghami, A survey of antiprion compounds reveals the prevalence of non-PrP molecular targets, J. Biol. Chem. 286 (2011) 27718–27728. https://doi.org/10.1074/jbc.M111.234393.
- [40] S. Gemma, G. Kukreja, P. Tripaldi, M. Altarelli, M. Bernetti, S. Franceschini, L. Savini, G. Campiani, C. Fattorusso, S. Butini, Microwave-assisted synthesis of 4-quinolylhydrazines followed by nickel boride reduction: a convenient approach to 4-aminoquinolines and derivatives, Tetrahedron Lett. 49 (2008) 2074–2077. https://doi.org/10.1016/j.tetlet.2008.01.128.
- [41] Y. Kawasaki, K. Kawagoe, C. Chen, K. Teruya, Y. Sakasegawa, K. Doh-ura, Orally administered amyloidophilic compound is effective in prolonging the incubation periods of animals cerebrally infected with prion diseases in a prion strain-dependent manner, J. Virol. 81 (2007) 12889–12898. https://doi.org/10.1128/JVI.01563-07.
- [42] K.T. Adjou, R. Demaimay, C.I. Lasmézas, M. Seman, J.-P. Deslys, D. Dormont, Differential effects of a new amphotericin B derivative, MS-8209, on mouse bse and scrapie: implications for the mechanism of action of polyene antibiotics, Res. Virol. 147 (1996) 213–218. https://doi.org/10.1016/0923-2516(96)89651-8.

- [43] D.A. Kocisko, A.L. Engel, K. Harbuck, K.M. Arnold, E.A. Olsen, L.D. Raymond, D. Vilette, B. Caughey, Comparison of protease-resistant prion protein inhibitors in cell cultures infected with two strains of mouse and sheep scrapie, Neurosci. Lett. 388 (2005) 106–111. https://doi.org/10.1016/j.neulet.2005.06.053.
- [44] Lakshmi Miller-Vedam and Sina Ghaemmaghami, Strain Specificity and Drug Resistance in Anti-Prion Therapy, Curr. Top. Med. Chem. 13 (2013) 2397–2406. https://doi.org/10.2174/15680266113136660168.
- [45] P.K. Baral, M. Swayampakula, M.K. Rout, N.N.V. Kav, L. Spyracopoulos, A. Aguzzi, M.N.G. James, Structural Basis of Prion Inhibition by Phenothiazine Compounds, Structure. 22 (2014) 291–303. https://doi.org/10.1016/j.str.2013.11.009.
- [46] H.-E. Kang, Y. Mo, R. Abd Rahim, H.-M. Lee, C. Ryou, Prion Diagnosis: Application of Real-Time Quaking-Induced Conversion, BioMed Res. Int. 2017 (2017) 5413936–5413936. https://doi.org/10.1155/2017/5413936.
- [47] S. Ghaemmaghami, B.C.H. May, A.R. Renslo, S.B. Prusiner, Discovery of 2-aminothiazoles as potent antiprion compounds, J. Virol. 84 (2010) 3408–3412. https://doi.org/10.1128/JVI.02145-09.
- [48] M.L. Bolognesi, H.N. Ai Tran, M. Staderini, A. Monaco, A. López-Cobeñas, S. Bongarzone, X. Biarnés, P. López-Alvarado, N. Cabezas, M. Caramelli, P. Carloni, J.C. Menéndez, G. Legname, Discovery of a Class of Diketopiperazines as Antiprion Compounds, ChemMedChem. 5 (2010) 1324–1334. https://doi.org/10.1002/cmdc.201000133.
- [49] U.S. Herrmann, A.K. Schütz, H. Shirani, D. Huang, D. Saban, M. Nuvolone, B. Li, B. Ballmer, A.K.O. Åslund, J.J. Mason, E. Rushing, H. Budka, S. Nyström, P. Hammarström, A. Böckmann, A. Caflisch, B.H. Meier, K.P.R. Nilsson, S. Hornemann, A. Aguzzi, Structure-based drug design identifies polythiophenes as antiprion compounds, Sci. Transl. Med. 7 (2015) 299ra123. https://doi.org/10.1126/scitranslmed.aab1923.
- [50] J.W. Hyeon, S.Y. Kim, S.M. Lee, J. Lee, S.S.A. An, M.K. Lee, Y.S. Lee, Anti-Prion Screening for Acridine, Dextran, and Tannic Acid using Real Time–Quaking Induced Conversion: A Comparison with PrPSc-Infected Cell Screening, PLOS ONE. 12 (2017) e0170266. https://doi.org/10.1371/journal.pone.0170266.
- [51] S. Ghaemmaghami, M. Ahn, P. Lessard, K. Giles, G. Legname, S.J. DeArmond, S.B. Prusiner, Continuous quinacrine treatment results in the formation of drug-resistant prions, PLoS Pathog. 5 (2009) e1000673—e1000673. https://doi.org/10.1371/journal.ppat.1000673.
- [52] A.K. Ghose, T. Herbertz, R.L. Hudkins, B.D. Dorsey, J.P. Mallamo, Knowledge-Based, Central Nervous System (CNS) Lead Selection and Lead Optimization for CNS Drug Discovery, ACS Chem. Neurosci. 3 (2012) 50–68. https://doi.org/10.1021/cn200100h.
- [53] T. Terada, Y. Tsuboi, T. Obi, K. Doh-ura, S. Murayama, T. Kitamoto, T. Yamada, K. Mizoguchi, Less protease-resistant PrP in a patient with sporadic CJD treated with intraventricular pentosan polysulphate, Acta Neurol. Scand. 121 (2010) 127–130. https://doi.org/10.1111/j.1600-0404.2009.01272.x.
- [54] A. De Luigi, L. Colombo, L. Diomede, R. Capobianco, M. Mangieri, C. Miccolo, L. Limido, G. Forloni, F. Tagliavini, M. Salmona, The efficacy of tetracyclines in peripheral and intracerebral prion infection, PloS One. 3 (2008) e1888–e1888. https://doi.org/10.1371/journal.pone.0001888.
- [55] C. Korth, B.C. May, F.E. Cohen, S.B. Prusiner, Acridine and phenothiazine derivatives as pharmacotherapeutics for prion disease, Proc. Natl. Acad. Sci. U. S. A. 98 (2001) 9836–9841. https://doi.org/10.1073/pnas.161274798.
- [56] S. Bongarzone, M.L. Bolognesi, The concept of privileged structures in rational drug design: focus on acridine and quinoline scaffolds in neurodegenerative and protozoan diseases, Expert Opin. Drug Discov. 6 (2011) 251–268. https://doi.org/10.1517/17460441.2011.550914.
- [57] E. Uliassi, L.E. Peña-Altamira, A.V. Morales, F. Massenzio, S. Petralla, M. Rossi, M. Roberti, L. Martinez Gonzalez, A. Martinez, B. Monti, M.L. Bolognesi, A Focused Library of